THE UNIVERSITY OF MANITOBA

LIBRARY

AUTHOR ... CHEUNG, Franklin C. T. .....

TITLE ... EFFECT OF MOLYBDENUM AND NIOBIUM CONTENT ON THE POLARIZATION BEHAVIOR OF COBALT-CHROMIUM ALLOY .....

THESIS ... M.Sc., 1985 .....

I, the undersigned, agree to refrain from producing, or reproducing, the above-named work, or any part thereof, in any material form, without the written consent of the author:

.....

THE UNIVERSITY OF MANITOBA

EFFECT OF MOLYBDENUM AND NIOBIUM CONTENT ON THE POLARIZATION BEHAVIOR OF COBALT-CHROMIUM ALLOY

by

Franklin C. T. Cheung

A THESIS

SUBMITTED TO THE FACULTY OF GRADUATE STUDIES

IN PARTIAL FULFILMENT OF THE

REQUIREMENTS FOR THE DEGREE OF

MASTER OF SCIENCE

DEPARTMENT OF MECHANICAL ENGINEERING

WINNIPEG, MANITOBA

July 1984

THE UNIVERSITY OF MANITOBA

FACULTY OF GRADUATE STUDIES

The undersigned certify that they have read a Master's thesis entitled: Effect of Molybdenum and Niobium Content on the Polarization Behavior of Cobalt-Chromium Alloy

submitted by: Franklin C. T. Cheung

in partial fulfillment of the requirements for the degree of Master of Science

The Thesis Examining Committee certifies that the thesis (and the oral examination, if required) is:

Approved [X] Not Approved [ ]

Dr. J. R. Cahoon J.R. Cahoon
Advisor

Date April 26, 1985

EFFECT OF MOLYBDENUM AND NIOBIUM CONTENT ON THE POLARIZATION BEHAVIOR OF COBALT-CHROMIUM ALLOY

BY

FRANKLIN C.T. CHEUNG

A thesis submitted to the Faculty of Graduate Studies of the University of Manitoba in partial fulfillment of the requirements of the degree of

MASTER OF SCIENCE

ACKNOWLEDGEMENT

The financial support of the National Science & Engineering Research Council of Canada in the form of an operating grant and student assistantship is gratefully acknowledged. I am also indebted to Dr. J. R. Cahoon under whose guidance this thesis was prepared.

TABLE OF CONTENTS

List of Tables

List of Figures

CHAPTER ONE INTRODUCTION

Metallic orthopaedic surgical implants have been employed for repairing the human skeletal system for many years. The first recorded use of metals came in 1550 with the use of gold wires as sutures. In the 1800s there were numerous reports of metal plates and pins to fix broken bones. In this century, especially in the last few decades, advancements in the field of materials and surgery have enabled the surgeon literally to rebuild many parts of the human body (1).

In choosing the materials for surgical implants, the effect of the implant on the body and the effect of the body on the implant has to be considered. In examining the effect of the implant on the body, the characteristics of the material that must be examined are (2):

1. Toxic or irriattional qualities of the material or its breakdown products to the molecular level, or additives incorporated into the material.
2. Mechanical characteristics of the material.
3. Fabricatability of the material into the desired implant form.
4. Sterilizability of the material.
5. Stability.
6. Size and shape of the material (tissue level).
7. Surface structure of the material.
8. Possible antigenicity of the material.
9. Thrombogenicity.
10. Antileukotaxis (infection prodisposition).
11. Carcinogenesis.

In examining the effect of the body on the implant, the material must be examined for changes such as (2):

1. Dissolution (i.e. degradation).
2. Changes in mechanical properties.
3. Wear particles.
4. Molecular structure (i.e. crosslinking in polymers and phases in alloys).

5. State of hydration.
6. Elution of low molecular weight of species.
7. Surface form.
8. General corrosion, crevice corrosion, and crack propagation.
9. Protein saturation on oxidation of the surfaces.
10. Cellular ingrowth.
11. Calcification.

The primary interest of this study is on the effect of the body on the crevice corrosion behavior of the implant.

The most common implant alloys used today are stainless steel and Co-Cr alloys. Both alloys are acceptable (but not ideal) in the physiological environment since metallic materials are always susceptible to corrosion to a certain extent. Previous studies show that stainless steels have high strength and ductility but do not have sufficient corrosion resistance, especially in the physiological environment (3). Co-Cr alloys generally have superior corrosion resistance but do not always have enough strength. The major problem with stainless steel as an implant material is its high susceptibility to crevice corrosion (20). Cobalt-chromium alloys generally exhibit better resistance to crevice corrosion but some such corrosion has been observed.

It is well-known that the addition of molybdenum to stainless steels will improve the pitting corrosion and crevice corrosion resistance. Therefore, an investigation was initiated to determine the effect of molybdenum content on the corrosion resistance of cobalt-chromium base alloys.

CHAPTER TWO CORROSION

2.1 General

All metals are susceptible to corrosion when in contact with body fluid. The extent of corrosion is one of the major factors that determines the acceptability of the implant. The most common types of corrosion are uniform, galvanic, pitting and crevice corrosion.

Corrosion is an electrochemical process which involves two distinct chemical reactions and which are dependent on each other. First there is the anodic reaction, where metal atoms turn into positively charged metal ions and go into solution leaving an excess amount of electrons on the metal surface. A second reaction, namely, the cathodic reaction is required to use up the excess electrons which are produced by the anodic reaction. Hence, the overall charge of the metal itself remains neutral. Thus electrons flow from anodic area to cathodic area through the metal, and continuous corrosion occurs.

The most common types of anodic reactions are:

1. $M \longrightarrow M^{+z} + ze^{-}$ (Metal dissolution or Oxidation)

The most common types of cathodic reactions are:

1. $2H^{+} + 2e^{-} \longrightarrow H_2$ (Hydrogen evolution)
2. $O_2 + 4H^{+} + 4e^{-} \longrightarrow 2H_2O$ (Oxygen reduction - acid solution)
3. $O_2 + 2H_2O + 4e^{-} \longrightarrow 4OH^{-}$ (Oxygen reduction - basic or neutral solutions)
4. $M^{+} + e^{-} \longrightarrow M$ (Metal deposition)
5. $M^{++} + e^{-} \longrightarrow M^{+}$ (Metal ion reduction)

Fig. 1 illustrates the electrochemical reactions involve in a typical corrosion process.

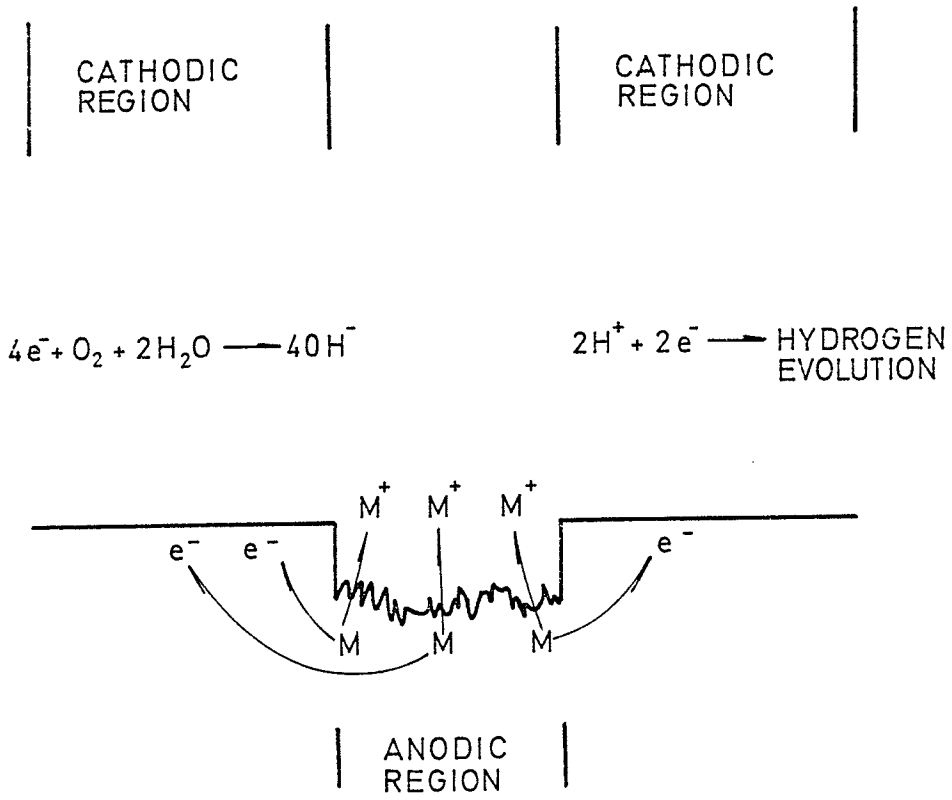

Fig. 1 Schematic representation of a corrosion process on a metal surface

Pitting and crevice corrosion are among the most damaging types of corrosion. These two types of corrosion can often be found in surgical implants, and they represent some of the major problems facing the implant designer today.

2.1.1 Crevice Corrosion

Crevice corrosion occurs in areas where free mixing and convection is limited. It can be found in localized sites such as lap joints, area under bolts and nuts, gasket surfaces, etc.

To illustrate the basic mechanism of crevice corrosion, consider a riveted plate section (Fig. 2) of metal M immersed in aerated seawater (pH = 7) (4).

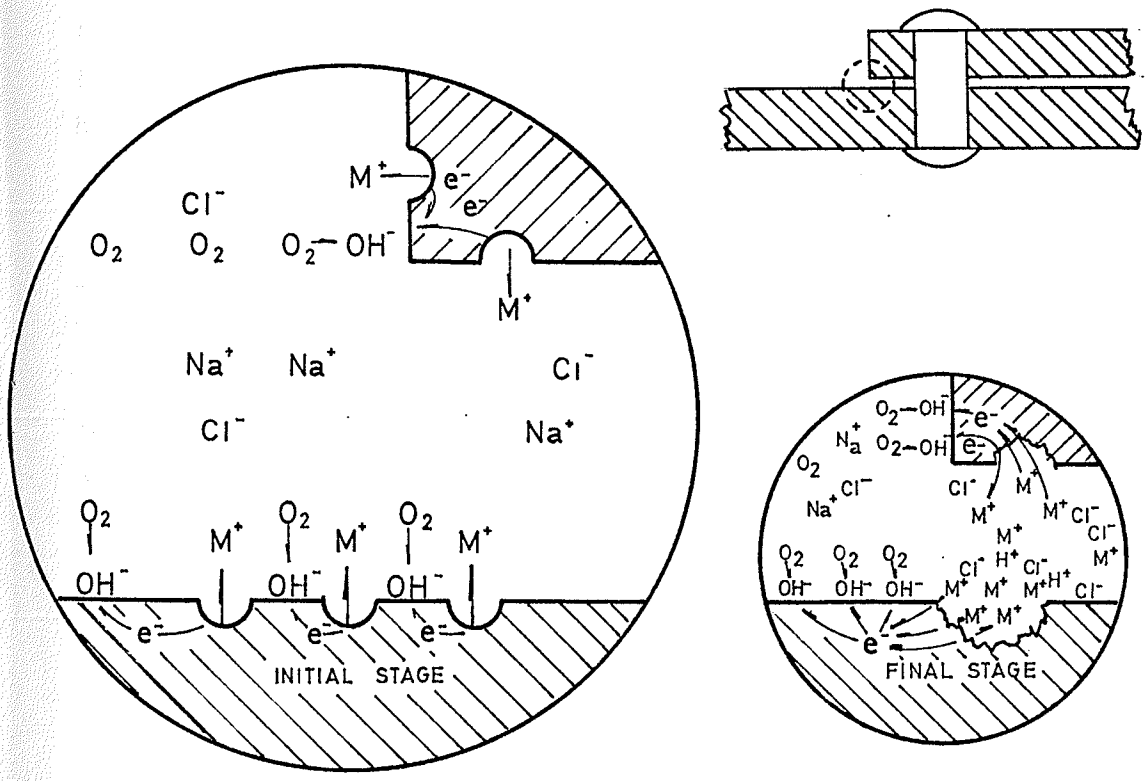

Fig. 2 Schematic representation of crevice corrosion in aerated seawater (pH = 7)

The anodic and cathodic reactions are as follow:

Anodic reaction : $M \longrightarrow M^+ + e^-$

Cathodic reaction: $O_2 + 2H_2O + 4e^- \longrightarrow 4OH^-$

During the initial stage, corrosion occurs uniformly over the entire surface, including the interior of the crevice (Fig. 2). After a short while, the oxygen concentration inside the crevice decreases due to the limited convection. Once the oxygen is used up in the crevice, the cathodic reaction in the crevice is no longer possible. Since the crevice area is insignificant compared to the exposed surface, the overall rate of corrosion remains unchanged. As anodic dissolution proceeds in the crevice, more and more positive metal ions go into solution inside the crevice. As a result, excessive positive charge inside the crevice attracts free chloride ions into the crevice and metal ions combine with chloride ions to form metal chloride. The metal chlorides of all transition metals hydrolize in water. The reaction is indicated as below,

$$M^+Cl^- + H_2O \longrightarrow MOH \downarrow + H^+Cl^-$$

which means metal chlorides react with water to form insoluble metal hydroxide and hydrochloric acid. The presence of hydrogen and chloride ions in the crevice accelerates the corrosion rate of most metals and alloys because the local acidity increases drastically. While the pH of the bulk solution is around 7, the pH inside the crevice can be as low as 2 or 3.

As anodic dissolution continues at an increasing rate inside the crevice, the oxygen reduction rate on the adjacent surfaces also increases which cathodically protects the external surfaces. This type of corrosion reaction is autocatalytic since the reaction itself is self-initiated; i.e. once the corrosion starts, it continues at an ever-increasing rate.

2.1.2 Pitting Corrosion

Pitting corrosion is one of the most damaging forms of corrosion. It perforates metal and alloys with only a small amount of metal dissolution and weight loss. This type of corrosion is a localized

and intense form of corrosion, and failures often occur unpredictably. Pits usually grow in the direction of gravity. Pitting requires an induction period ranging from months to years before pits can initiate. However, once pits are initiated, they penetrate metal in an ever-increasing rate.

The mechanisms of crevice corrosion and pitting corrosion are basically the same. Both are caused by differential aeration which is a result of limited convection. However, the initiation processes of crevice and pitting corrosion are different. The former type initiates by the presence of the crevice which results in differential aeration. The latter type initiates by a locally high dissolution rate because of surface defects such as an emerging dislocation, stacking faults, etc. This high dissolution rate produces an excessive positive charge which draws chloride ions (For a NaCl solution) into the initiation site. The presence of chloride ions accelerates the corrosion rate. As a result, a pit is formed and further dissolution at an ever-increasing rate is caused by differential aeration.

Both crevice and pitting corrosion are autocatalytic. The basic difference between crevice and pitting corrosion is that pitting corrosion creates its own crevice (pits). Therefore, metals and alloys susceptible to pitting corrosion are also susceptible to crevice corrosion although the reverse is not always true.

2.2 Polarization and Passivation

2.2.1 Polarization

An electrochemical reaction is said to be polarized if the rate of reaction is retarded by various physical and chemical factors. In corrosion, there are two types of polarization, activation polarization and concentration polarization.

Activation polarization results from the sequential delay of the electrochemical reaction at the interface of metal and electrolyte. For example: hydrogen evolution, which is one of the cathodic reactions, can be envisaged as a process possessing a number of steps. First, electrons transfer from the anodic region to the cathodic region. Second, hydrogen ions transport to the metal-electrolyte interface. Third, hydrogen ions combine with electrons to form hydrogen atoms. Fourth, hydrogen atoms fuse into hydrogen bubbles and the hydrogen evolution process is completed. If any of these processes is hindered or delayed, the process is said to be activation polarized.

Concentration polarization results from the aggregation of ions near the metal surface which slows down the diffusion process of further migration of ions. Again, consider the case of hydrogen reduction. As the cathodic reaction proceeds, more and more hydrogen ions are drawn near the metal-electrolyte interface. As a result, the concentration of hydrogen ions builds up forming layers near the metal surface. This in turn draws the negative ions (e.g. chloride ions) near the hydrogen ions' layers leading to the formation of an electrical double layer. This electrical double layer acts as a barrier to the diffusion process. In other words, concentration polarization is controlled by the diffusion process.

2.2.2 Passivation

A metal or alloy is said to be passivated if its corrosion rate is considerably lower than the rate corresponding to thermodynamical equilibrium. The slowing down of the anodic reaction, or passivation, mainly results from the formation of a passive layer on the metal surface which reduces the ionic conductivity of the electrochemical reaction.

The presence of a passive layer on metal was found many years ago. The earliest experiment was performed by Faraday who immersed a piece of iron in concentrated nitric acid and found no reaction between the iron and the acid. Then, he diluted the solution by adding water to it but again there was no reaction. But when he scratched the surface of the metal with a glass rod, a violent reaction resulted. This experiment is a classic example which demonstrates the presence of passive layer.

During the past decade, the development of surface analytical techniques such as Auger Electron Spectroscopy, Low Energy Electron Diffraction, X-ray Spectroscopy etc. has enabled material scientists to analyse the surface composition of solid surfaces. With the aid of these techniques, it has been found that the passive layers on the metal surface, in almost all cases, are oxide films. These oxide films can slow down the corrosion rate considerably. Therefore, the presence of this passive layer on metal surface is beneficial in most alloys. A number of alloys which exhibit good corrosion resistance possess a stable oxide layer. Hence, the mechanism of oxide formation and growth, and the mechanism of breakdown of the oxide layer are the most important factors affecting the corrosion properties of almost all surgical implant alloys.

2.3 Development of an Oxide Layer and its Breakdown

2.3.1 Mechanism of oxide formation and oxide growth

There are two ways oxygen may react with metal surfaces, physical adsorption and chemical adsorption. Physical adsorption involves no chemical bond and the bonding is by Van der Waals forces. Chemical adsorption involves a chemical bond such as a covalent or ionic bond. Physical adsorption usually occurs on a partially oxidized surface where the first layer of partial layer forms by chemisorption. As uniform corrosion proceeds, electron transfer occurs uniformly over the surface. Oxygen ions in the solution or electrolyte are attracted

to the anodic sites where chemical bonds are formed between the oxygen ions and the substrate. Hence, the first or partial layer of oxide is formed by chemisorption (5).

There are three types of oxide, 1. nonconductive, 2. semiconductive, and 3. conductive. The electrical conductivity of the oxide layer is determined by the concentration of metal ions which diffuse into the layer. Most alloys develope a conductive layer in the initial stage of passivation and form the semiconductive or nonconductive layers at the final stage. The common type of carbon steel forms only a conductive oxide layer in aerated water or chloride solution. The ferrous and ferric ions diffuse into the layer continuously which results in continuous corrosion. Hence, the stability of the oxide film determines the susceptibility of the alloy to corrosion. For most good corrosion-resistance alloys, the oxide films are mostly non-conductive. The formation of this film is preceeding by the formation of a conductive and then a semiconductive layer.

The formation of oxide and its growth can be explained as follows. As corrosion proceeds on an alloy surface in an electrolyte, a flow of current or electrons occurs. As the rate of corrosion increases, the corrosion potential increases which results in the formation of an oxide film through a reaction of the type

$$M + H_2O \longrightarrow M\text{-}O + 2H^+ + 2e^-$$

This type of reaction leads to chemisorption of oxygen ions onto the metal surface.

The adsorption of oxygen by physical adsorption is mainly due to the fluctuation of electric dipole of the oxygen molecules and the slight electrical charge on the metal surface. In other words, the oxygen molecules are absorbed by the metal due to the slight electrical charges created by both the oxygen molecules

and the metal surface. The slight electrical charge on the metal surface is caused by the bombardment of free electrons upon the metal surface. The physically adsorbed layer is very weak and the heat of adsorption is low.

The formation of conducting oxide layers occurs when oxygen ions are attracted to the anodic site on the metal surface. At the same time, the metal ions diffuse into the layer forming a conductive layer of metal oxide. This process, so called the place exchange mechanism (6), governs the growth of conducting oxides.

The formation and growth of semi-conducting oxides is similar to that for conducting oxides except there are less metal ions diffused into the oxide layer which results in the semi-conducting behavior of the oxide layer.

The formation of a non-conducting oxide initiates by chemisorption and subsequent growth by physical adsorption. Further growth of the layer is achieved by the presence of an electric field. The presence of the electric field accelerates the passage of ions in the direction of the field. The thickness of the oxide growth depends on the total potential across the oxide (5).

2.3.2 Breakdown of passive layer

The chemical breakdown of oxide films requires a certain conditions before the proceeding of the breakdown (7):

1. A specific potential must be reached or exceeded. This is called the critical potential for pitting or the breakdown potential.

2. Damaging species (halides ions) are needed to initiate and propagate breakdown.

3. Existence of an induction time between the time of initiation of breakdown and completion of breakdown when pitting or crevice corrosion commences.

4. Breakdown occurs at highly localized sites.

There are three proposed models of breakdown which can satisfy the above requirements and common elements can be found in all three models.

I Adsorbed Ion Displacement Model

The presence of halide ions (e.g. Cl^-) promotes the breakdown by replacing the anions (oxygen ions) in the oxide film. The halide ions combine with the metal ions in the oxide layer and the oxide layer enters into solution. Once the layer is thinned breakdown will proceed 'explosively' at an ever-increasing rate. The displacement is highly localized and attack is more likely to occur at susceptible sites such as defects and inclusions.

II Ion Migration or Penetration Model

This model suggests that the breakdown is achieved by the penetration of damaging ions (halide) through the oxide film and which reach the metal-film interface. Various mechanisms of the Penetration Model have been suggested and only few will be discussed here. Richardson and Wood (8,9) suggest that there are always existing pores or defects in the film that allow instantaneous penetration of the halide ions through the film. Hoar, et al (10), suggest that halide ions enter the film without exchange with the anions to produce a contaminated site. A few contaminated sites migrate into the film and create a path of high conductivity which in turn produces an electric field around the path of migration. The electrostatic force created by the electric field causes the rupture of the film.

III Chemico-Mechanical Models

Three proposed mechanisms will be discussed here. Hoar (11) suggests that mutual repulsive forces are generated by absorbed halide ions on the surface of the film. When the repulsive forces are sufficient enough to rupture the film, damaging anions can attack the metal surface and breakdown proceeds. Sato (12) suggests that absorbed halide ions create an electric field and cause the film to rupture by the electrostriction pressure exceeding the compressive fracture strength of the film. Ambrose and Kruger (13), suggest that absorbed halide ions penetrate the film and react with the metal to form a low density product at the metal-film interface. This low density product eventually grows into a pocket under the film. As the pocket expands, stress is applied on the film directly above the pocket until the film cracks and breakdown is initiated.

2.4 Relationship between crevice corrosion and the cyclic polarization curve

The most common method of the evaluation of crevice corrosion susceptibility is by the in situ immersion method accomplished by measurement of weight loss. This method can take lengthy exposure times before actual weight loss starts. Noble metals and alloys can require years of time for the localized attack to develop or initiate. Electrochemical measurement has been employed for many years for evaluation of corrosion susceptibility and has proved successful in comparison with the immersion test.

Wilde and Williams (14) have made a significant advance in the development of evaluation procedures. They conducted anodic polarization measurements with several alloys that had been previously evaluated in seawater for more than four years.

A cyclic potentiodynamic anodic polarization measurement was employed which involved a potential scan in the noble direction until the anodic current reached 2000 ua/cm, whereby the scanning direction was reversed. Polarization curves obtained by this method exhibit two significant potentials. 1. The critical potential (E_c) or the pitting potential. 2. The protection potential (E_p) or the repassivation potential. It was found that the magnitude of the "difference potential" ($E_c - E_p$) can be correlated directly with the extent of crevice corrosion after more than four years in sea water (14, 15).

For alloys exhibiting active-passive behavior, the presence of hysterisis during cyclic polarization indicates susceptibility to crevice corrosion. Fig. 3 shows a schematic cyclic polarization curve. As shown in Fig. 3, region 1 to 2 indicates the metal suffers general corrosion or overall dissolution on the metal surface.

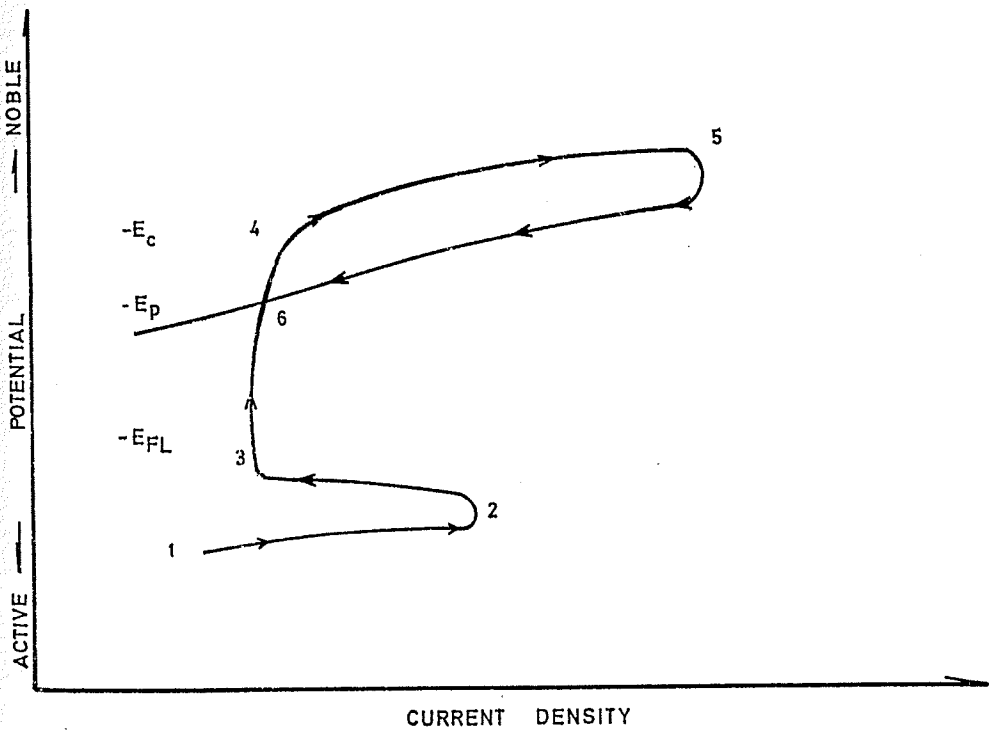

Fig. 3 Schematic Cyclic Polarization Curve for metal exhibiting active-passive behavior

Point 2 indicates the start of passivation as oxide layers begin to build up on the metal surface. At point 3, the Flade Potential, the metal is completely passivated. As the potential is increased, the metal suffers corrosion at a much slower rate than at the rest potential. As the potential reaches point 4, the critical potential, breakdown of the oxide film occurs and general corrosion resumes. At point 5, the reverse scan starts. From 5 to 6, the existing pits start to repassivate. At the point where the reverse and forward scan lines intersect, point 6, the potential is called the protection potential. The magnitude of protection potential depends on the extent of pit propagation. Wilde (15) has demonstrated the marked effect of pit propagation on the value of protection potential (Fig. 4). It is clear from Fig. 4 that the greater the extent of pit propagation the lower the protection potential. It is therefore important when using cyclic polarization studies to determine susceptibility to crevice corrosion to use the same maximum current value for each of the specimens.

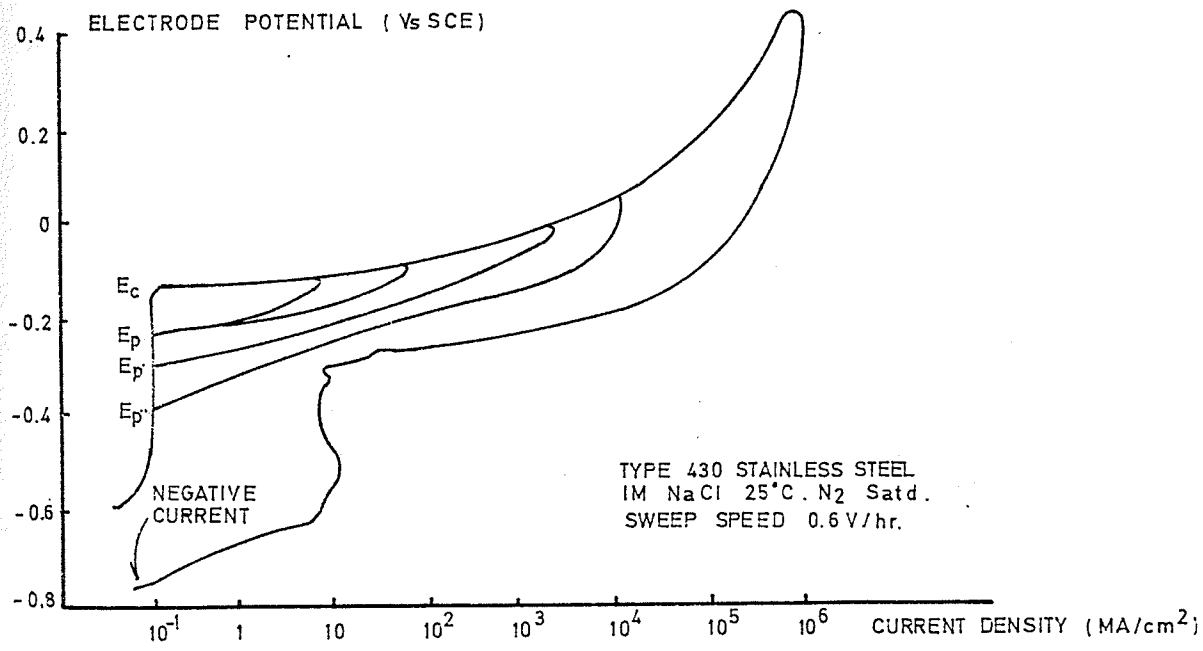

Fig. 4 Cyclic polarization behavior of Type 430 stainless steel in 1 M NaCl demonstrating the marked effect of pit propagation on protection potential

CHAPTER THREE EXPERIMENTATION

3.1 Specimen Preparation

All specimens were prepared by melting about 300 grams of alloy in a vacuum induction furnace and casting into cylindrical ingots about 20mm in diameter and 100mm long. The specimens were then machined into cylinders 10mm in diameter and 20mm long. One end of the specimens was then tapered from the perimeter toward the center at an angle of approximately 10 degree to ensure a good seal on the specimen holder (Fig. 5). A hole was then drilled in every specimen at the center of the tapered end. The specimens were then heat treated. The specimen compositions and heat treatment temperatures and times for all alloys tested are given in Table I.

Immediately after heat treatment, a piece of brass rod was forged into the hole of every specimen. Another hole was then drilled threaded on the brass portion. The specimen was then sanded to 600 grit paper and was finally cleaned in an ultrasonic cleaner and ethanol solution immediately prior to testing.

3.2 Experimental Set Up

The surface area of each specimen was determined by measuring all dimensions to the nearest 0.01mm. The area of the tapered face was not included. The specimen was then mounted on the electrode holder as shown in Fig. 5 (16). The specimen was then placed into a polarization cell together with the reference electrode (suturated calomel electrode or SCE) and counter electrodes (platinum electrodes) as shown in Fig. 5. Conduction between the reference electrode and the solution was achieved by a salt bridge connection. All alloys were tested in a 0.17 M saline solution buffered with 0.034 g/l of Na_2CO_3.

The solution was poured into the cell which was placed into a water bath regulated at a temperature of 37 C. The pH of the testing solution was adjusted to 7.4 $\pm$ 0.1 by the addition of 0.1 M NaOH or 0.1 M HCl.

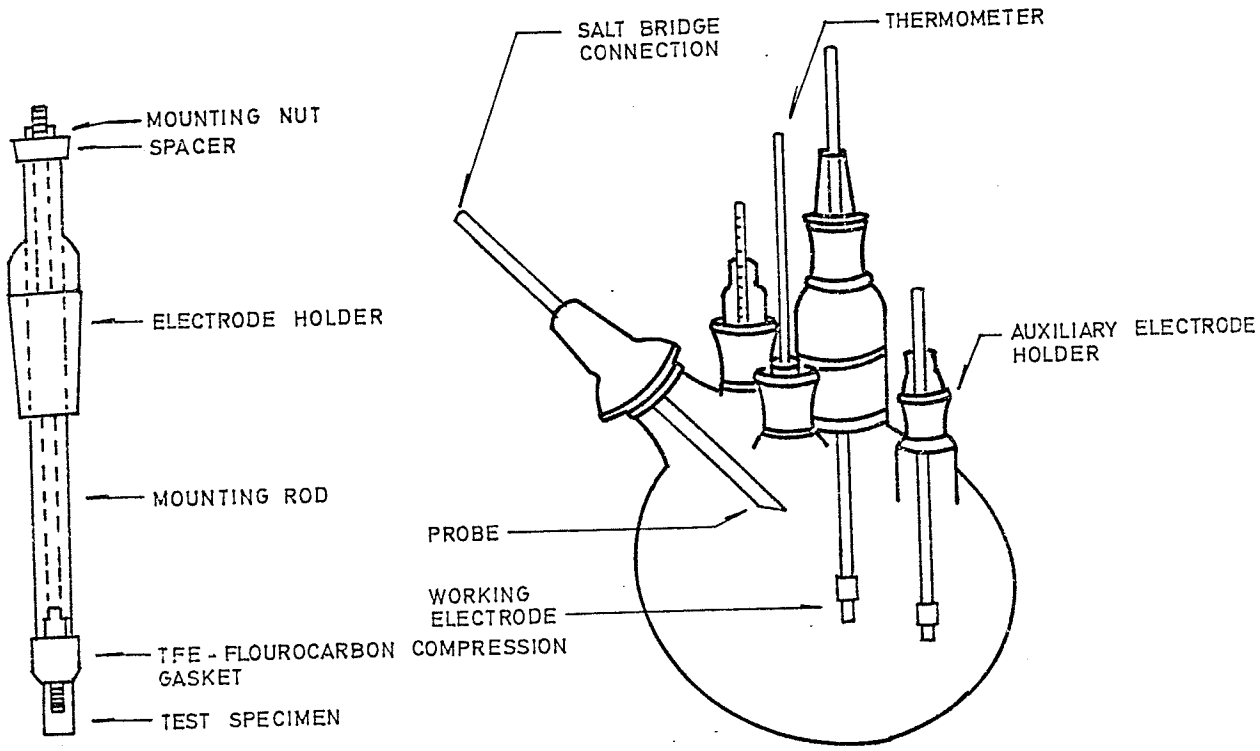

Fig. 5 Standard Recommended Electrode Holder and Polarization Cell

The specimen was allowed to stabilize in the solution for two hours before the polarization was started. After stabilization, the rest potential, E_r, was obtained and potentiodynamic polarization was started. Polarization curves were obtained by using a Wenking potentiostat (#68TS3) and an Erwin Halstrup motorpotentiometer (#MP165). The voltage scan rate was 600 mv/hr and the scan was reversed when the current density reached a value

approximately two decades higher than the breakdown potential. The current was monitored using a strip chart recorder. Fig. 6 shows the schematic potentiodynamic anodic polarization wiring diagram.

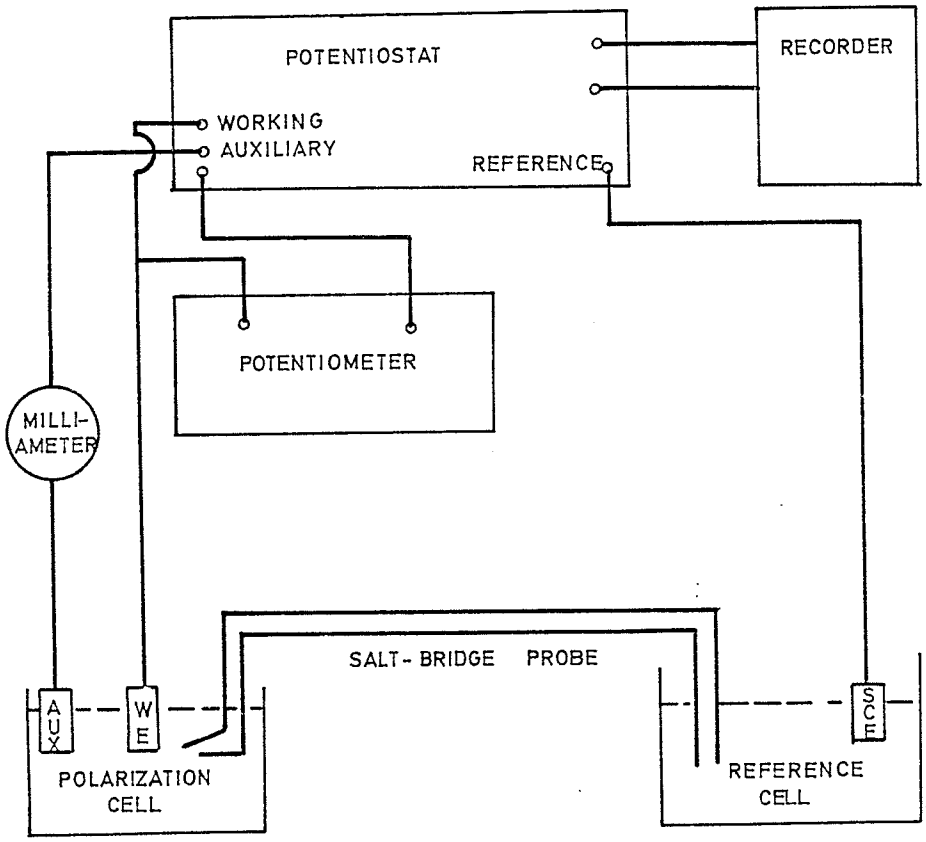

Fig. 6 Schematic wiring diagram for potentiodynamic anodic polarization test

3.3 Cyclic Potentiodynamic Polarization

After the specimen was placed in the polarization cell and stablized for two hours, the rest potential was recorded and the voltage scan was started at a rate of 600 mv/hr. The current was

recorded continuously and was converted into current density by simply dividing the current reading by the exposed surface area of the specimen. The scan was reversed when current density reached a value approximately two decades higher than the breakdown potential. The value of breakdown potential E_b and protection potential E_p were also recorded.

3.4 Surface Analysis by Auger Electron Spectroscopy

Auger Electron Spectroscopic analysis was performed by the Educational and Research Services of Carnegie-Mellon University who utilized a Physical Electronics Industries Thin Film Analyzer. Two specimens were submitted for this test, (1) Co-24%Cr-4.7%Mo, (2) Co-23%Cr-2.1%Mo. The specimens were both about 10 mm diameter and 2 mm in thickness. The specimens were sanded to 600 grit paper and then immersed for 6 hours in 0.17 M NaCl solution (pH = 7.4) buffered with 0.034 g/l of Na_2CO_3.

Sputtering of the specimen during Auger analysis was accomplished with a 2 kV ion beam and an initial current of 1 ma which was held for about 30 minutes after which the beam current was gradually increased to ensure that the bulk composition was reached. The element peaks which were monitored were Co (775 eV), Cr (571 eV), O (510 eV), C (272 eV) and Mo (221 eV). Complete spectra were taken prior to and periodically during sputtering.

CHAPTE FOUR RESULTS AND DISCUSSION

4.1 Results

A series of tests was conducted on Co - 25% Cr alloys containing 0 - 7% Mo, 1 - 5% Nb and 2.5% Nb - 5% Mo. The composition, heat treatment temperature and time for the alloys are given in Table I. Potentiodynamic polarization was conducted on all alloys. The results are plotted as polarization curves. For alloys containing 0 - 7% Mo, the polarization curves are shown in Fig. 7 to 12. Fig. 13 shows the effect of Mo content on the magnitude of Ec - Ep. For alloys containing 1 - 5% Nb, the polarization curves are shown in Figs. 14 to 22. For an alloy containing 2.5% Nb - 5% Mo, the polarization curve is shown in Fig. 23. Fig. 24 shows the effect of Mo content on the magnitude of E_c and E_p. Fig. 25 shows the effect of Nb content on the magnitude of E_c and E_p and Fig. 26 shows the effect of Nb content on the magnitude of $E_c - E_p$. All the significant potentials of each curve are given in Table II.

Two specimens were submitted for Auger Electron Spectroscopic Analysis. The composition profiles for the Co - 24% Cr - 4.7% Mo and Co - 23% Cr - 2.1% Mo are shown in Fig. 27 and Fig. 28. A complete spectrum prior to the start of sputtering is shown in Fig. 29 and a spectrum after 28 milliamp-minutes of sputtering is shown in Fig. 30.

TABLE I

Figure No.	Composition Co	Cr	Mo	Nb	Heat Treatment 1 Temp. K	Time Hrs.	Heat Treatment 2* Temp. K	Time Hrs.
7	Bal	26.1%	0%	0%	1423	96	--	--
8	Bal	25.6%	1%	0%	1423	96	--	--
9	Bal	22.8%	2.1%	0%	1423	96	--	--
10	Bal	24.8%	3.4%	0%	1423	96	--	--
11	Bal	23.8%	4.7%	0%	1423	96	--	--
12	Bal	23.1%	7.5%	0%	1423	96	--	--
14*	Bal	26%	0%	1.21%	1423	96	1473	48
15	Bal	26%	0%	1.21%	1423	96	--	--
16	Bal	25.2%	0%	2.2%	1423	96	--	--
17*	Bal	25.2%	0%	2.2%	1423	96	1473	48
18*	Bal	26.4%	0%	2.75%	1423	96	1473	48
19	Bal	26.4%	0%	2.75%	1423	96	--	--
20*	Bal	24.7%	0%	4.0%	1423	96	1473	48
21	Bal	24.7%	0%	4.0%	1423	96	--	--
22*	Bal	24.7%	0%	4.0%	1423	96	1473	48
23	Bal	25%	5%	2.5%	1423	96	--	--

* Heat treatment 2 was employed for Solution treatment of Niobium Carbide which was found in the microstructure of the specimen after Heat treatment 1.

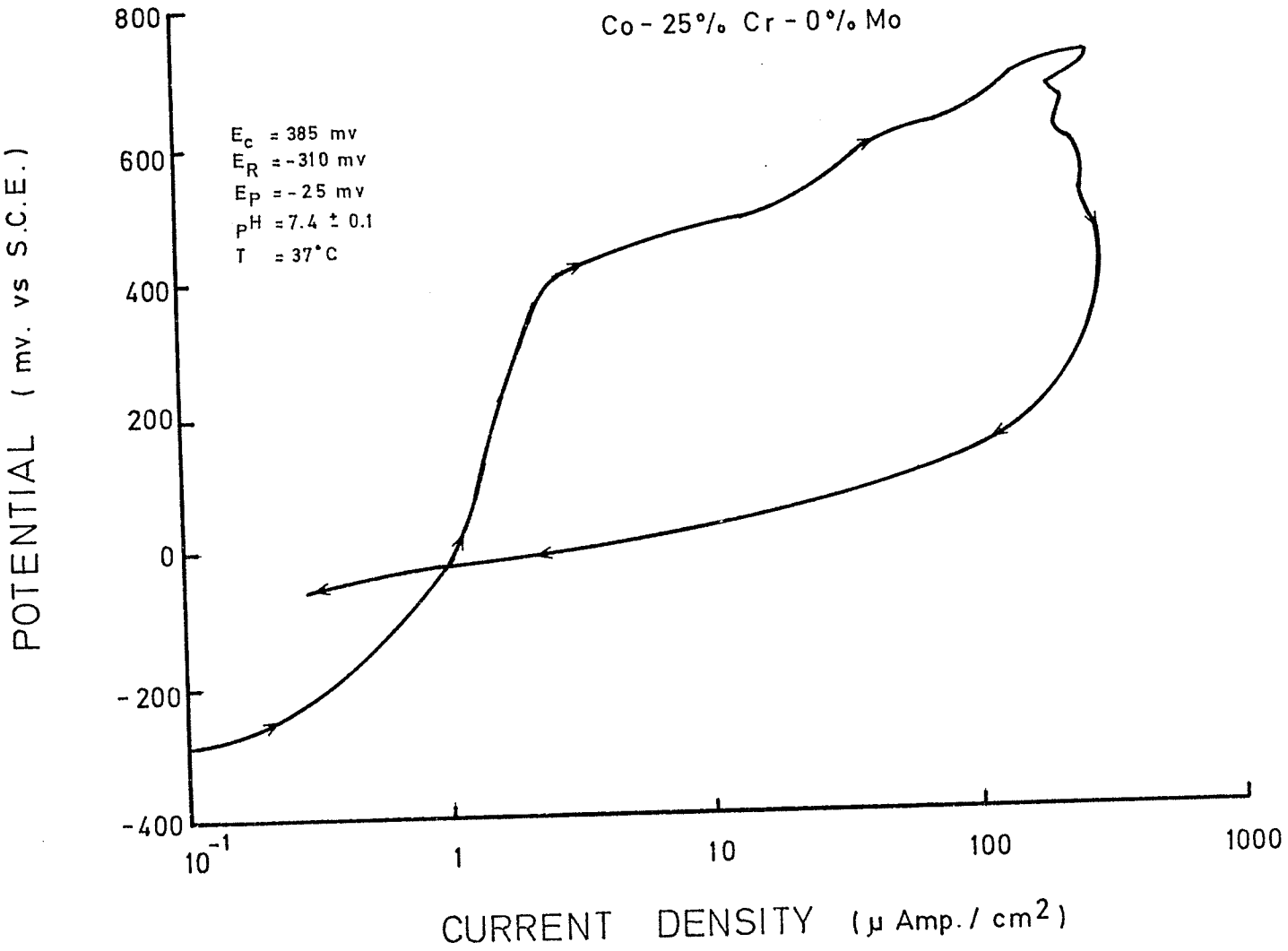

Fig. 7. Polarization curve for Co-25%Cr-0%Mo

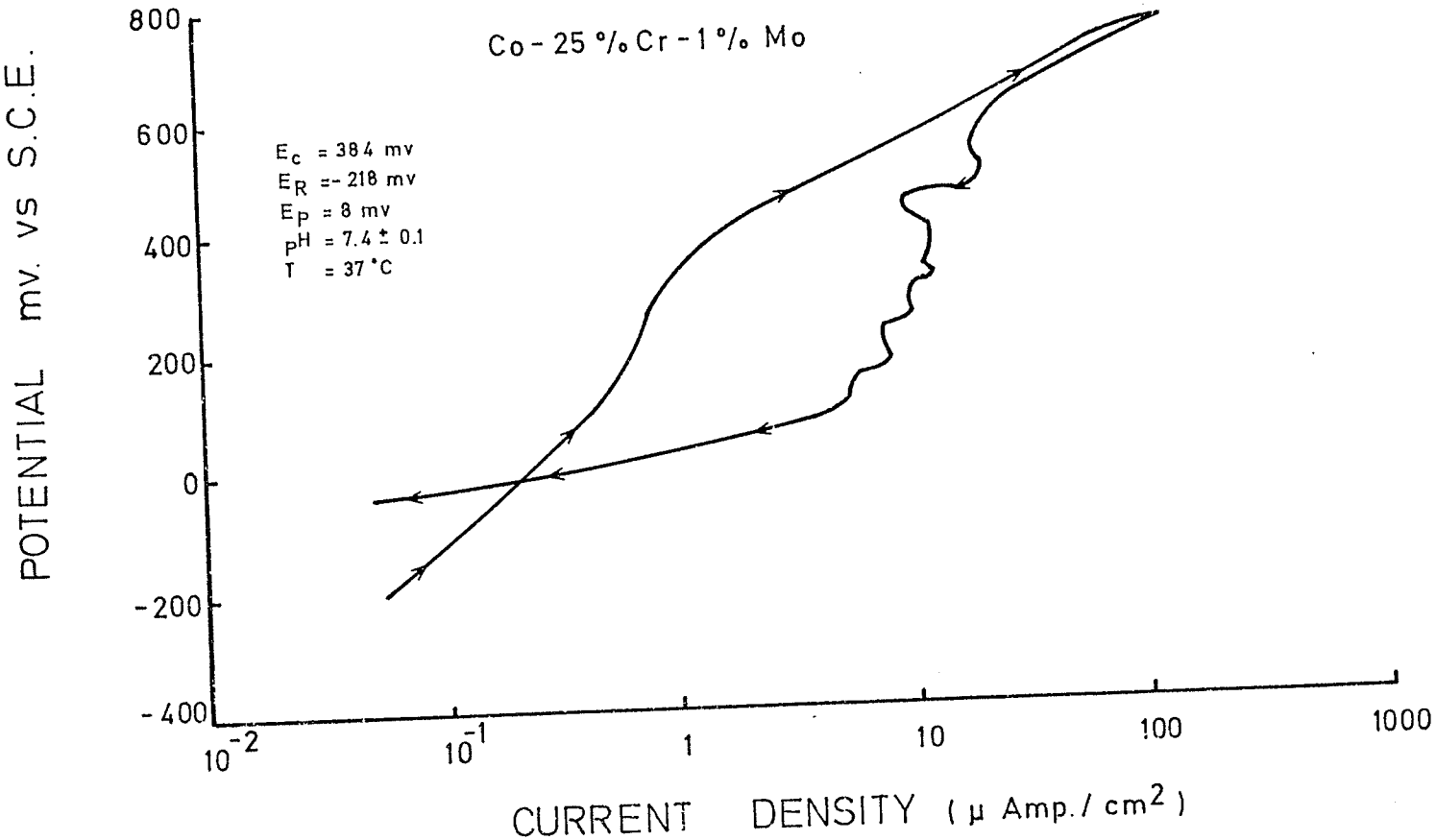

Fig. 8. Polarization curve for Co-25%Cr-1%Mo

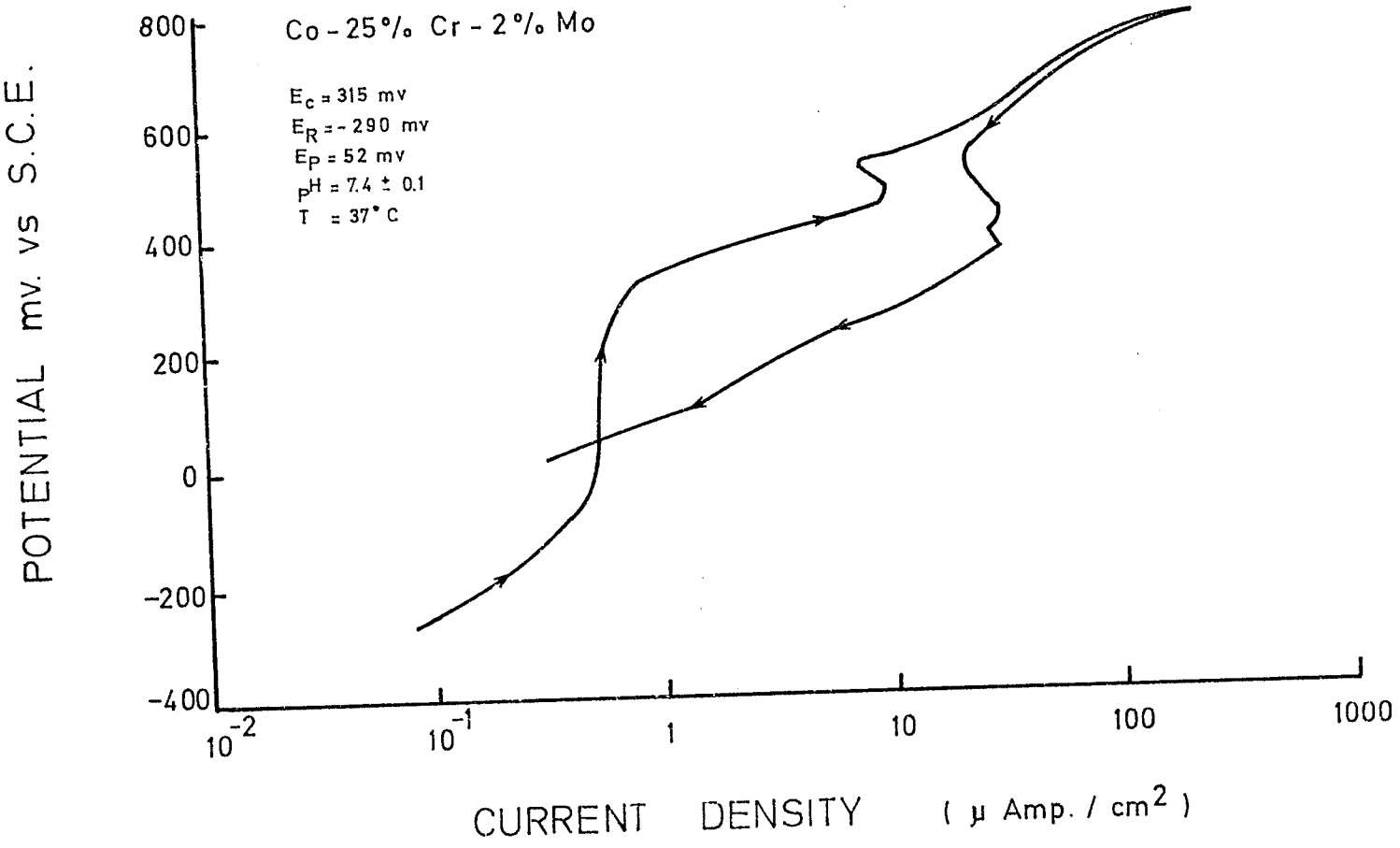

Fig. 9. Polarization curve for Co-25%Cr-2%Mo

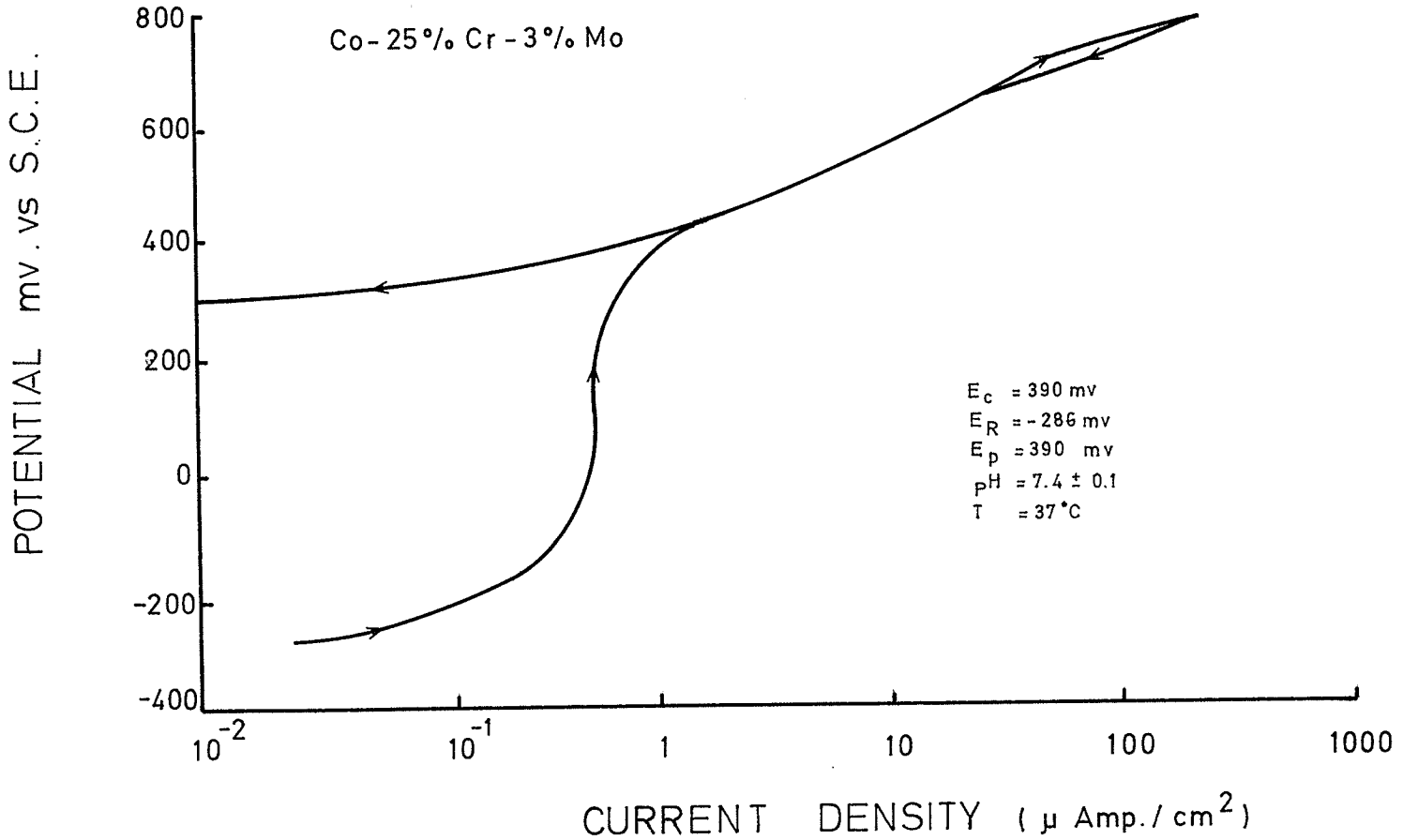

Fig. 10. Polarization curve for Co-25%Cr-3%Mo

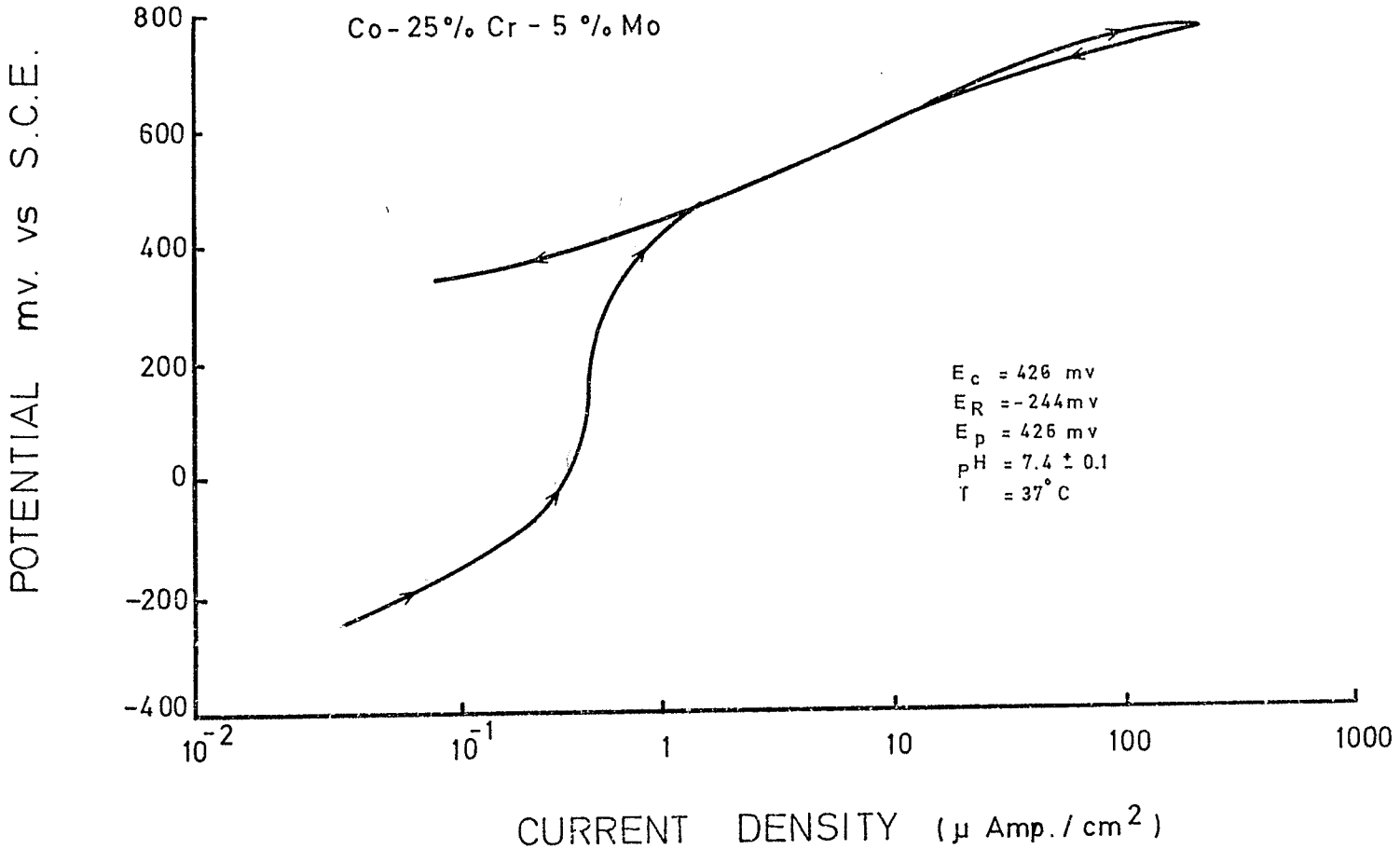

Fig. 11. Polarization curve for Co-25%Cr-5%Mo

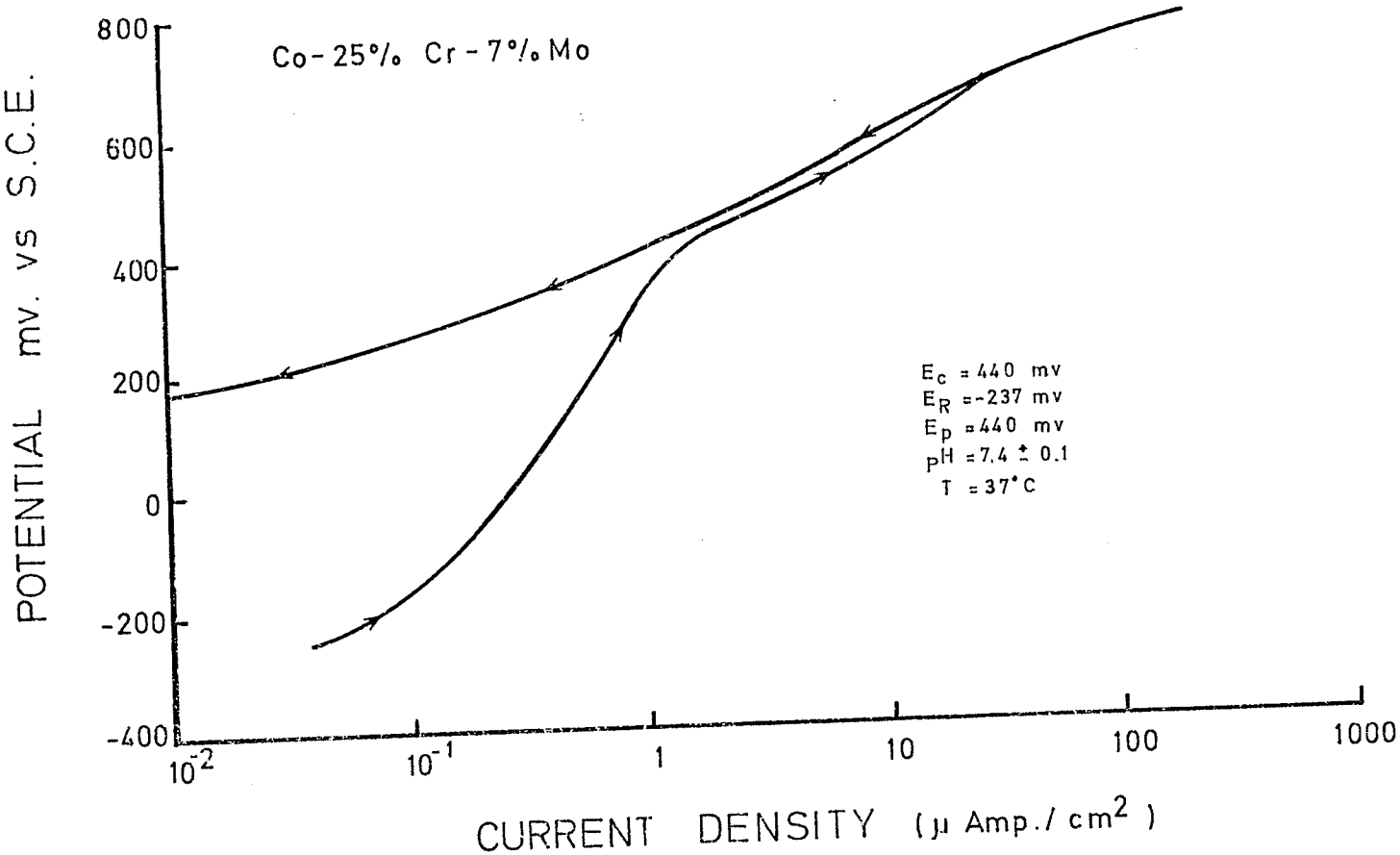

Fig. 12. Polarization curve for Co-25%Cr-7%Mo

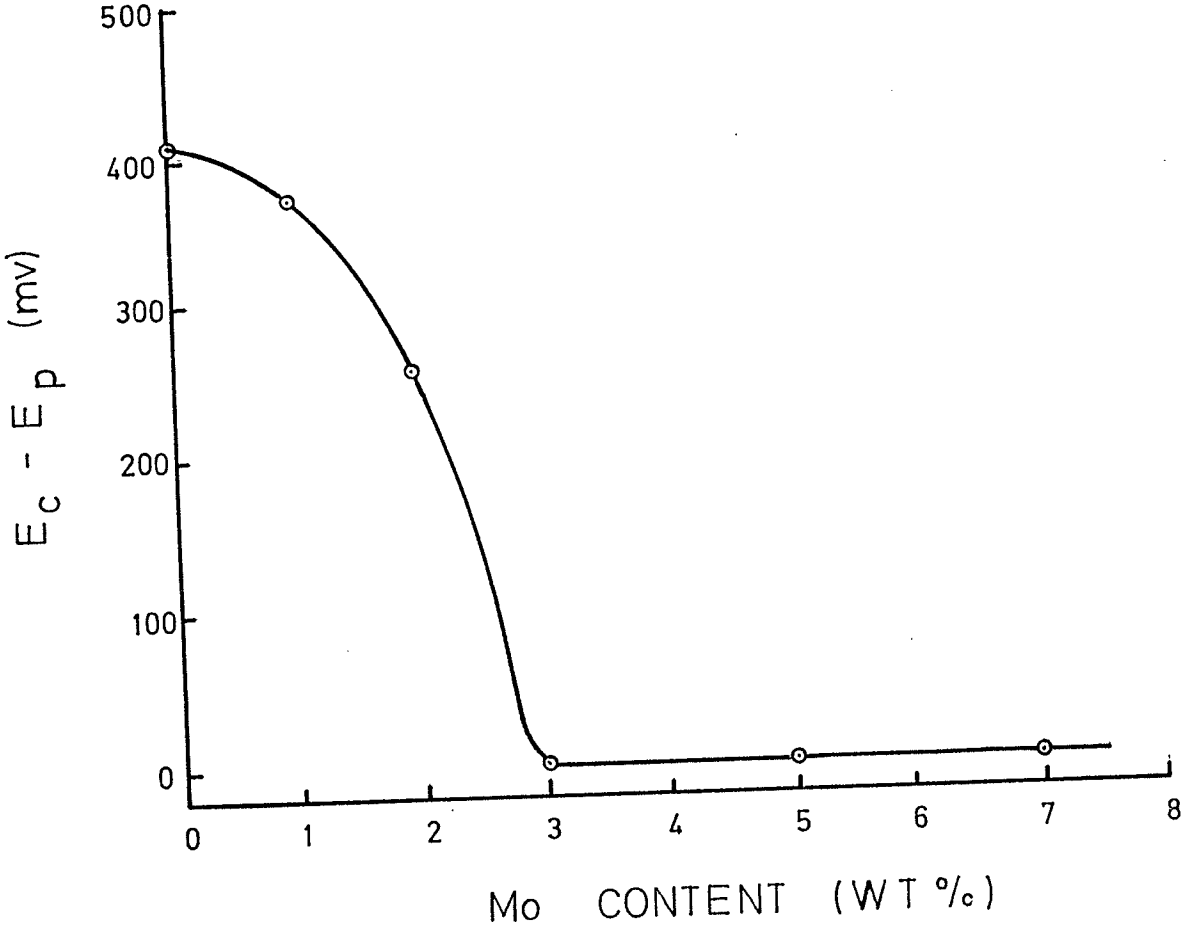

Fig. 13. Effect of Mo content on the value of $E_c - E_p$

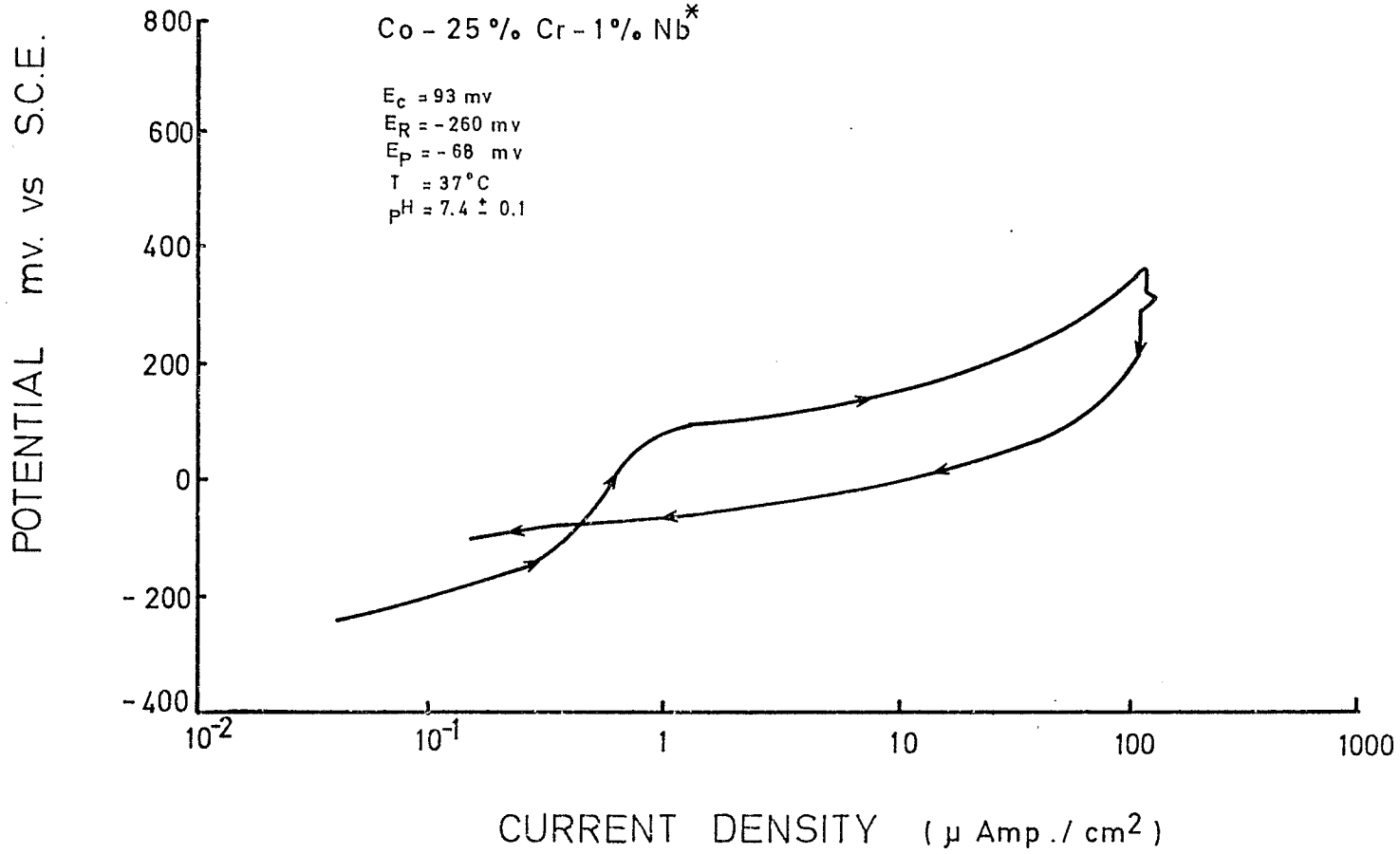

Fig. 14. Polarization curve for Co-25%Cr-1%Nb*

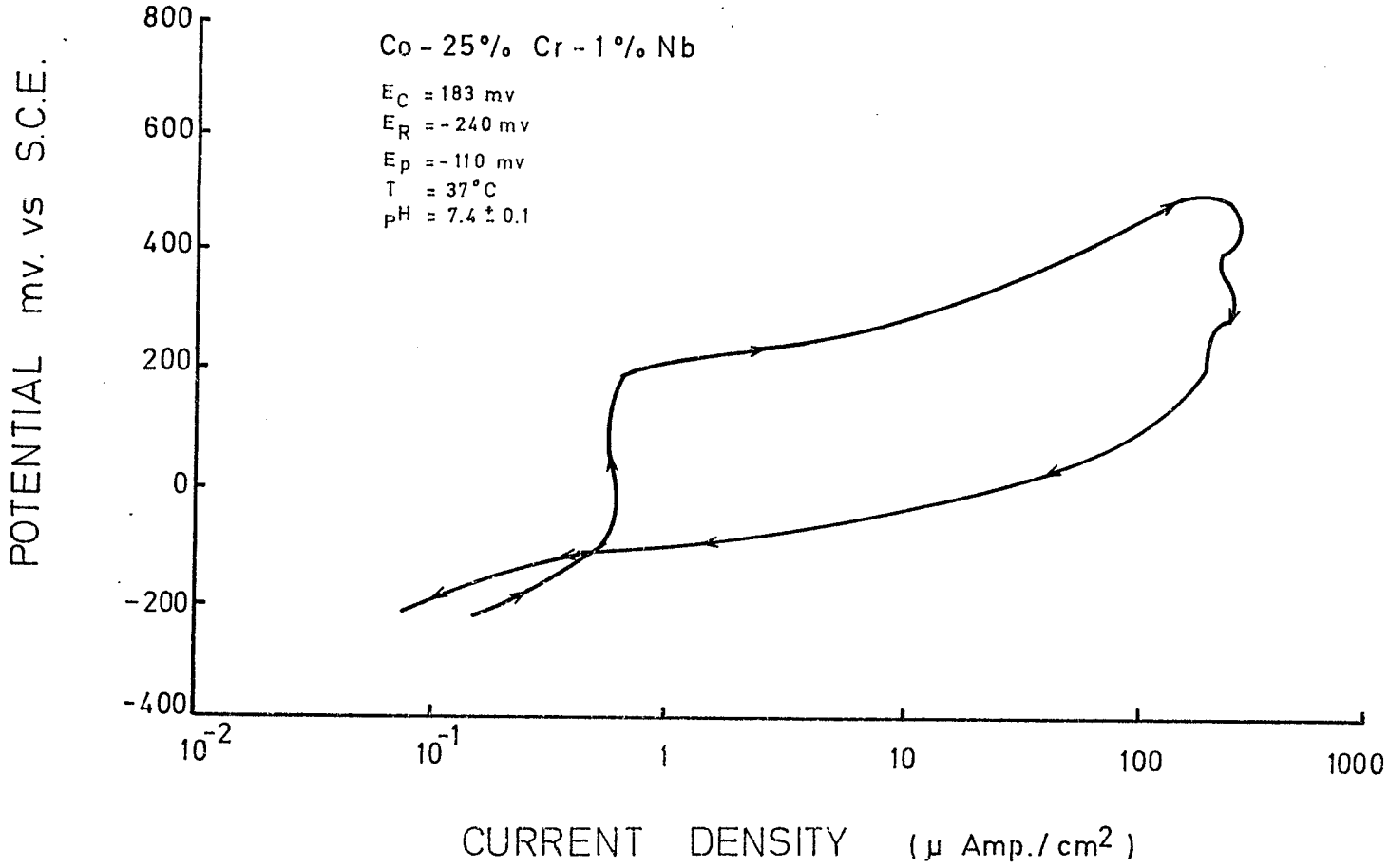

Fig. 15. Polarization curve for Co-25%Cr-1%Nb

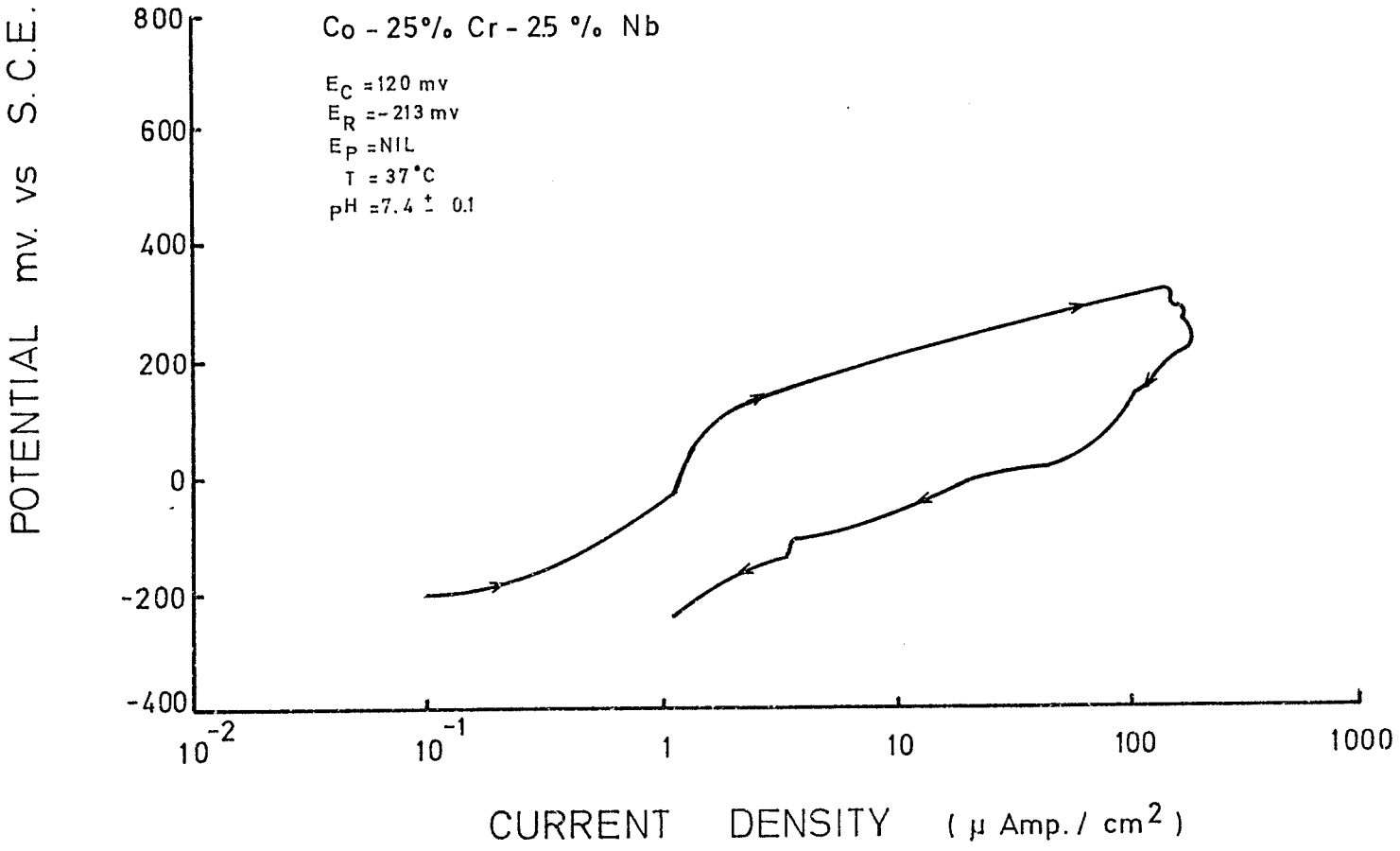

Fig. 16. Polarization curve for Co-25%Cr-2.5%Nb

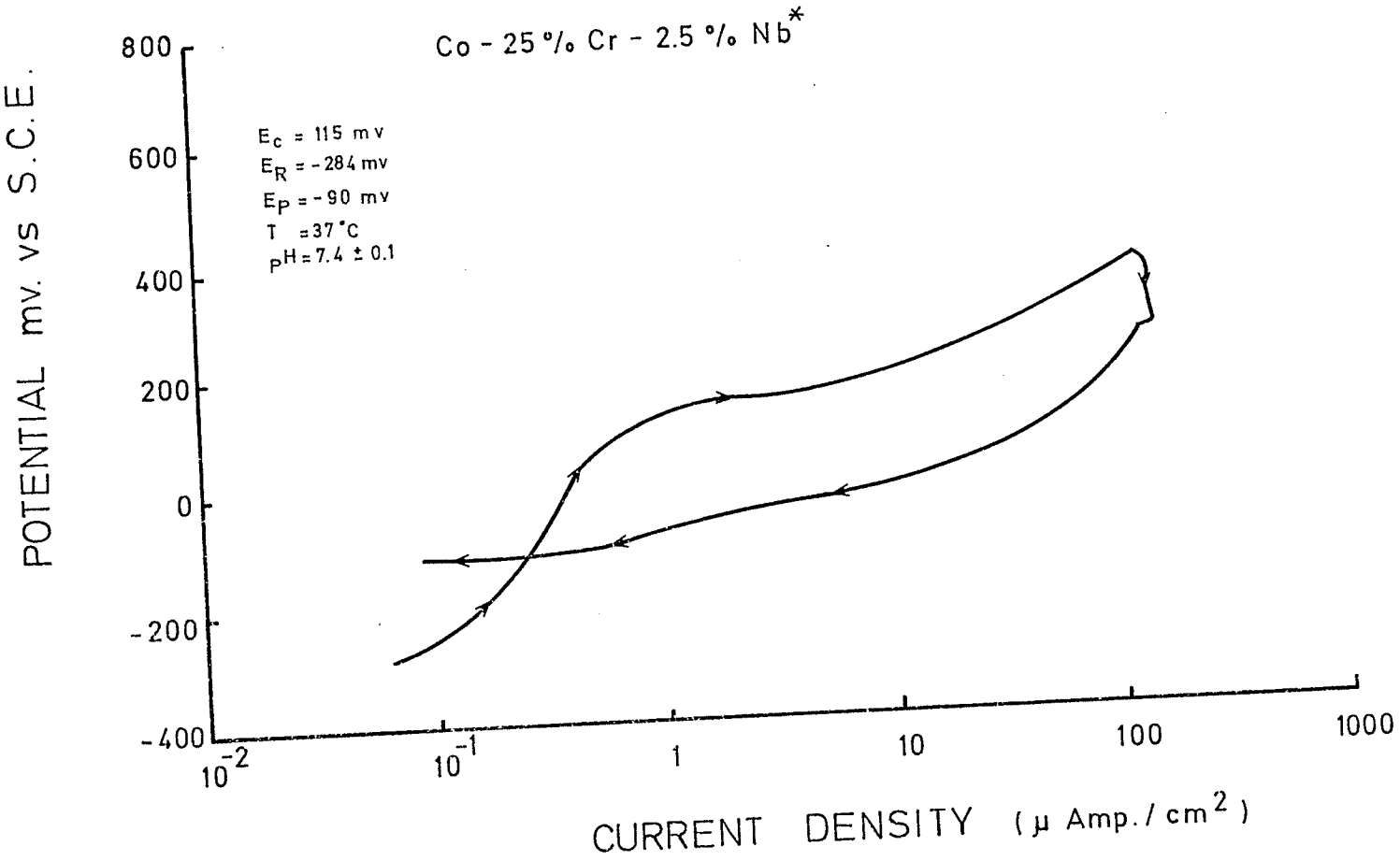

Fig. 17. Polarization curve for Co-25%Cr-2.5%Nb*

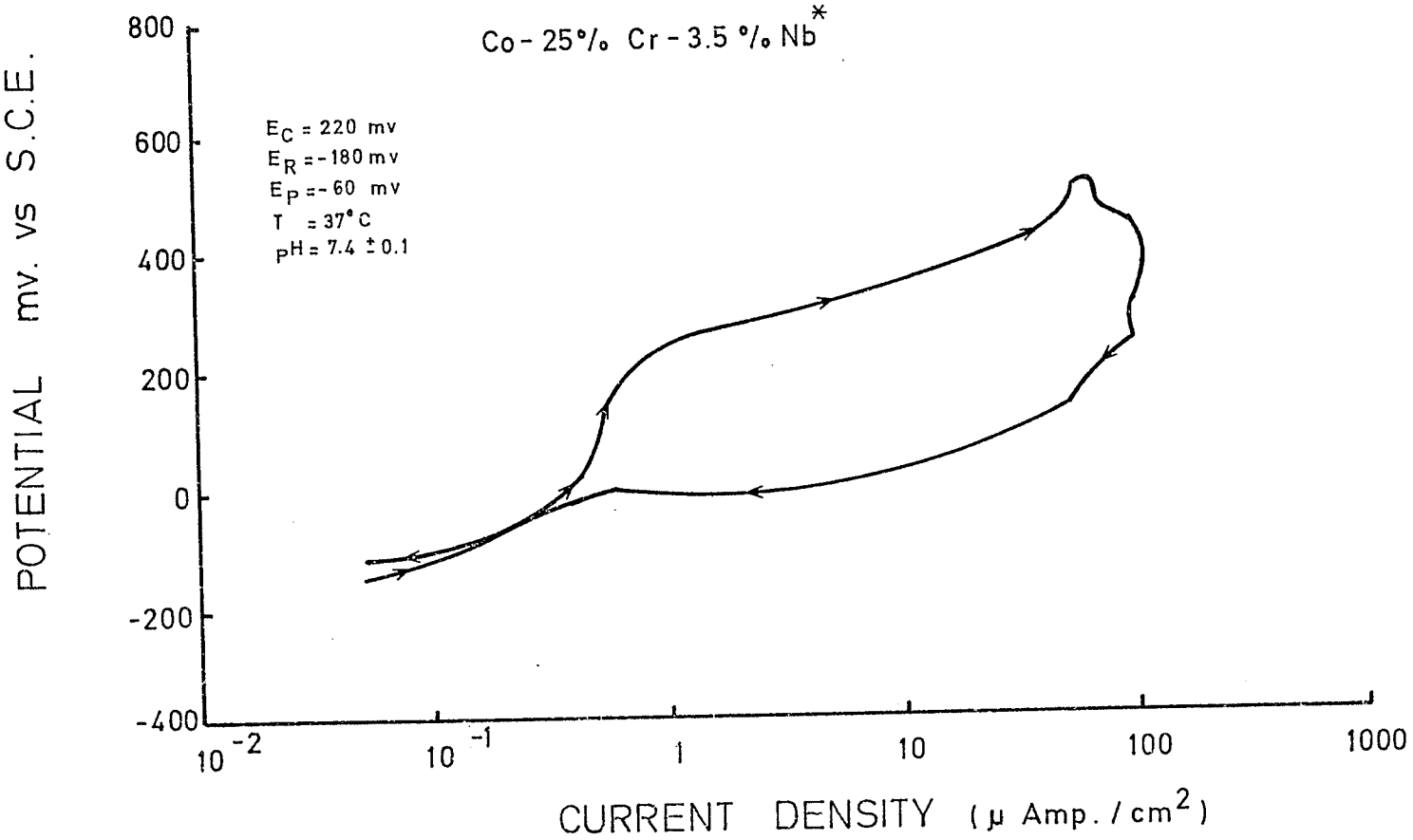

Fig. 18. Polarization curve for Co-25%Cr-3.5%Nb*

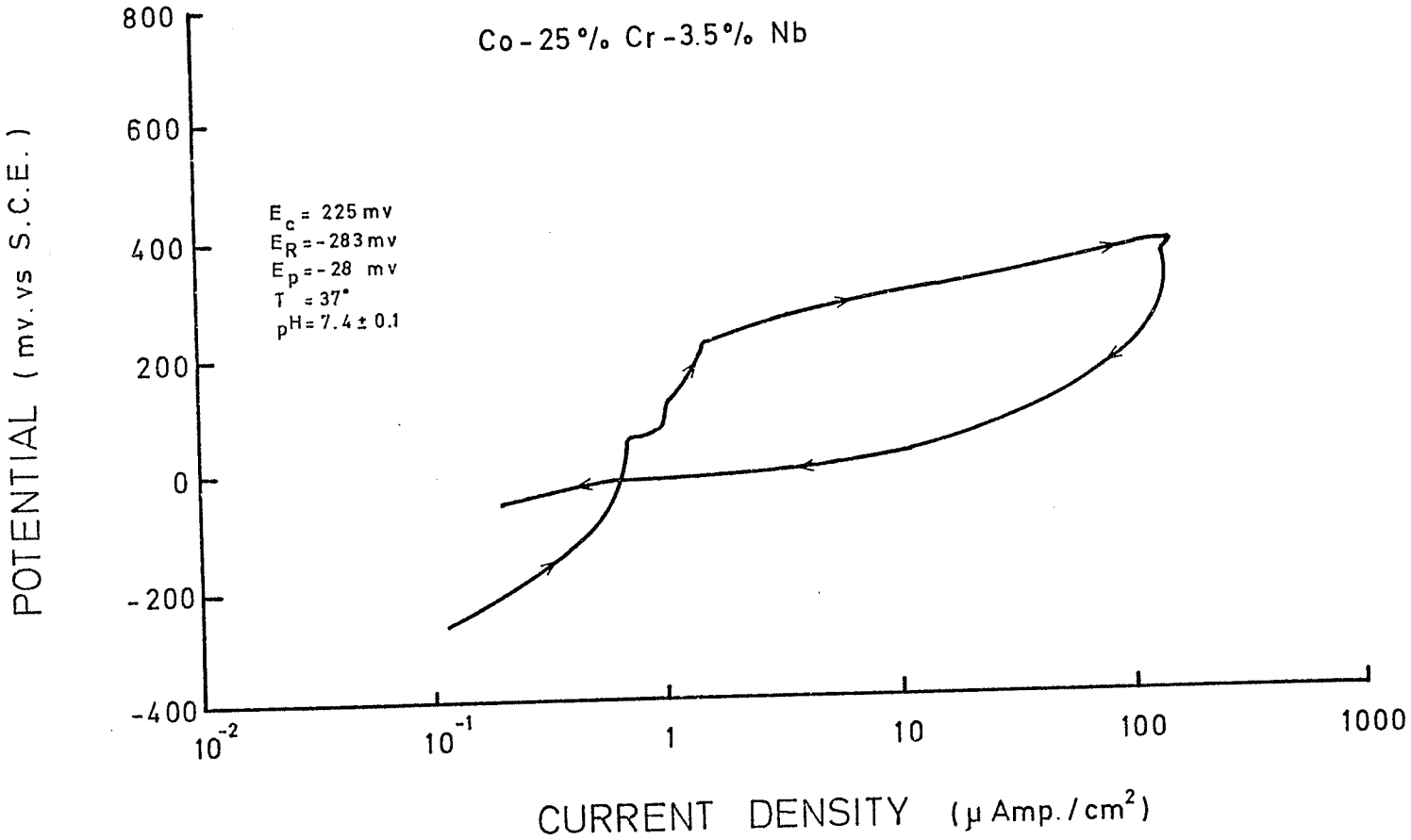

Fig. 19. Polarization curve for Co-25%Cr-3.5%Nb

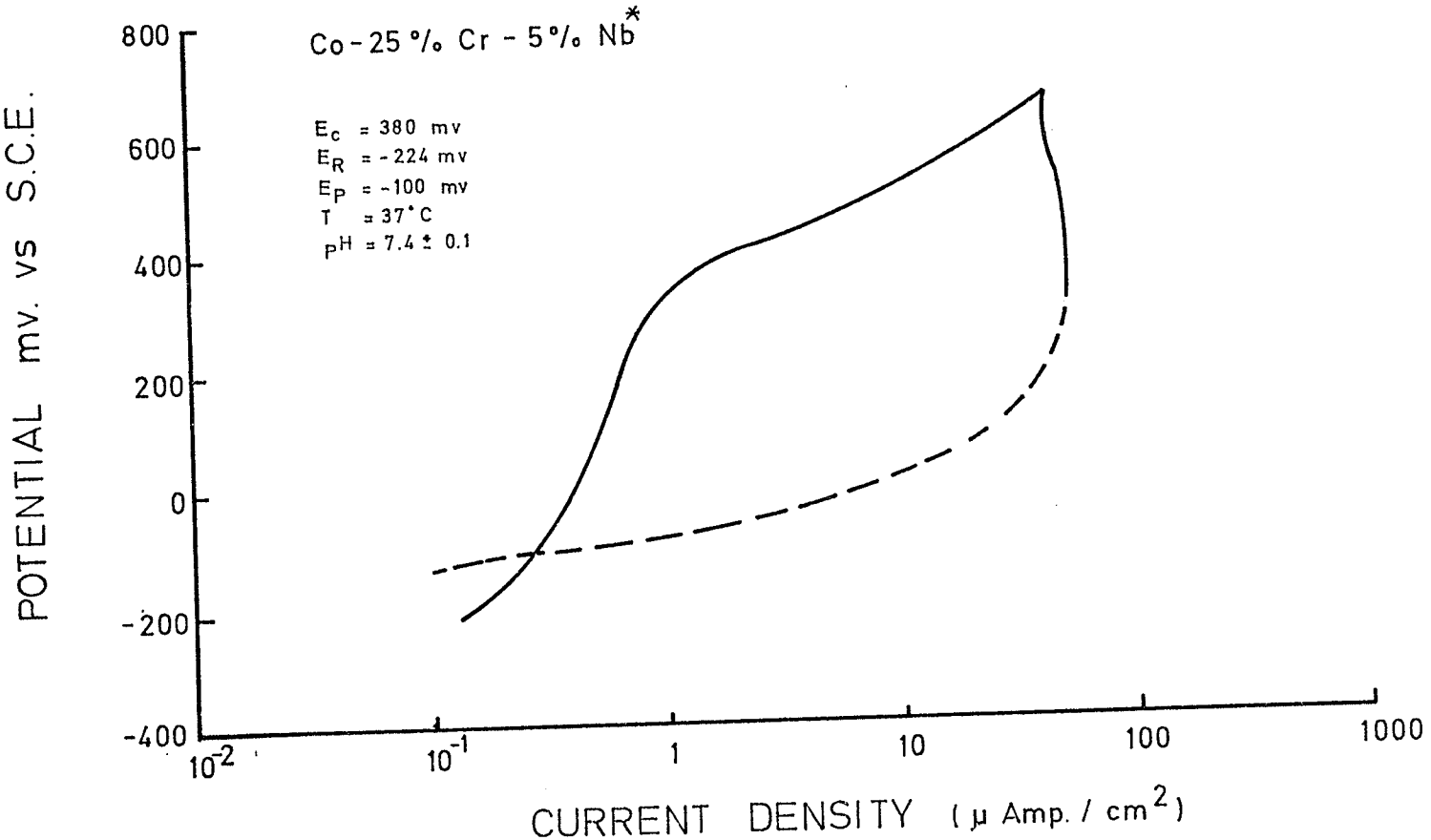

Fig. 20. Polarization curve for Co-25%Cr-5%Nb*

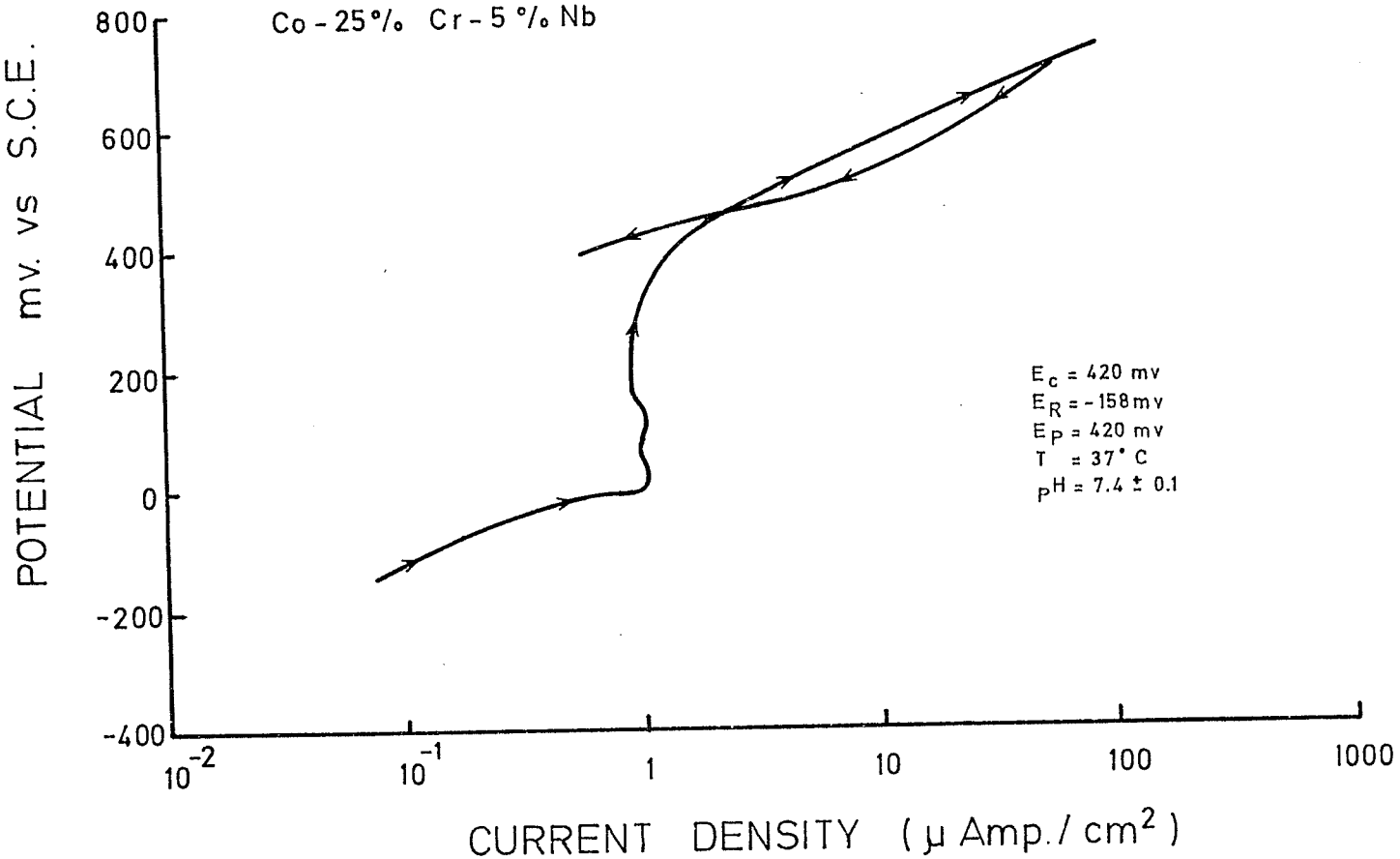

Fig. 21. Polarization curve for Co-25%Cr-5%Nb

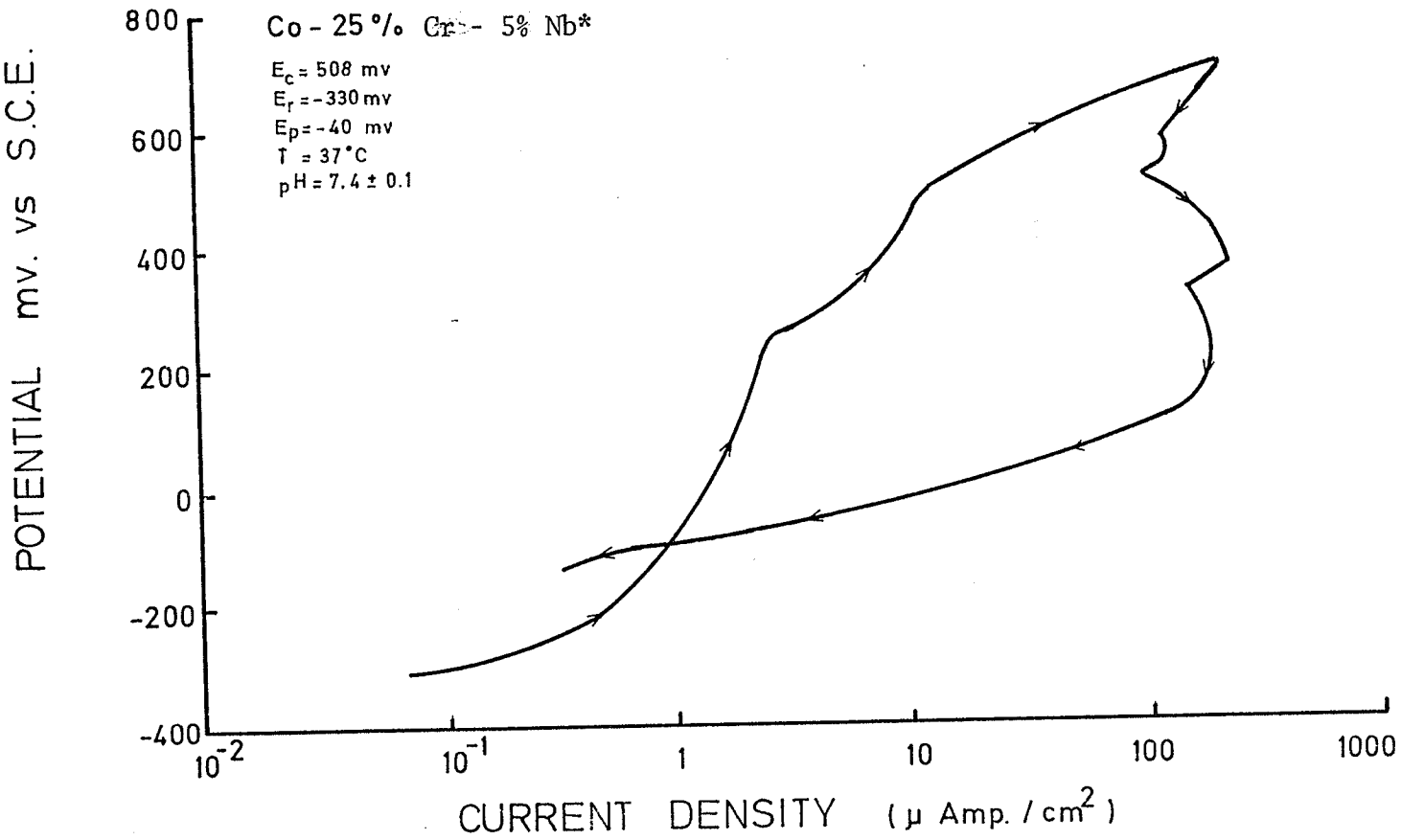

Fig. 22. Polarization curve for Co-25%Cr-5%Nb*

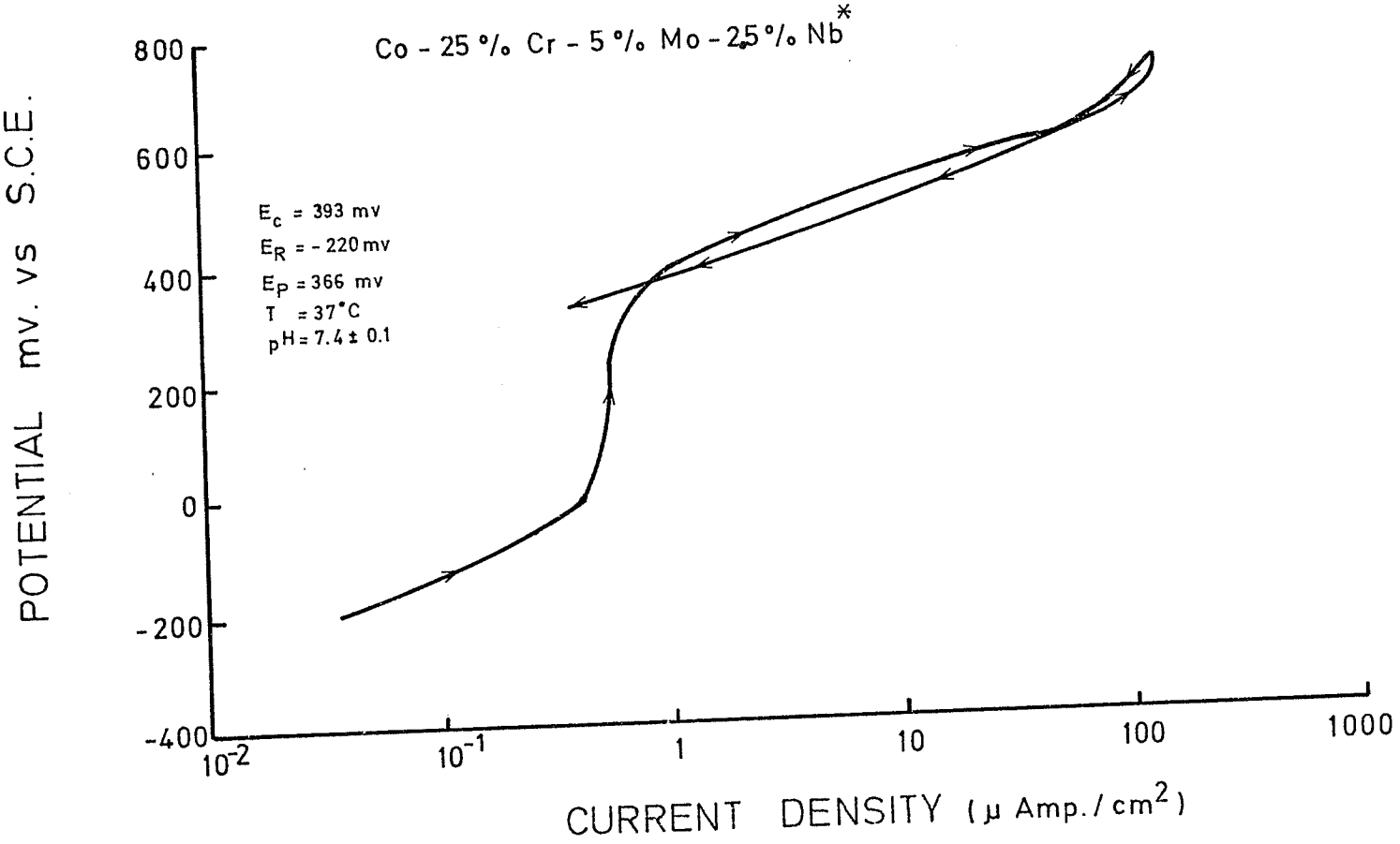

Fig. 23. Polarization curve for Co-25%Cr-5%Nb

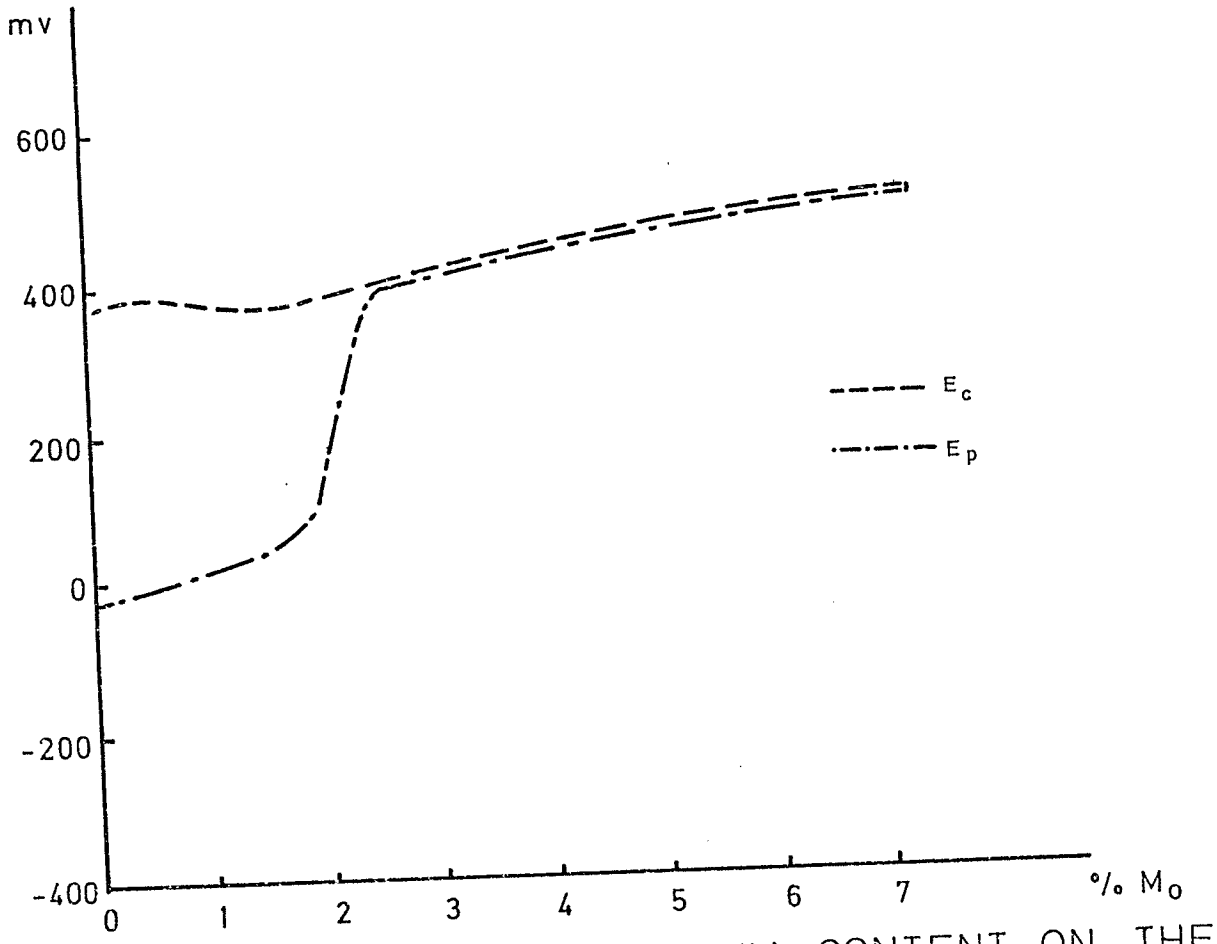

Fig. 24. EFFECT OF MOLYBDENUM CONTENT ON THE MAGNITUDE OF E_c AND E_p

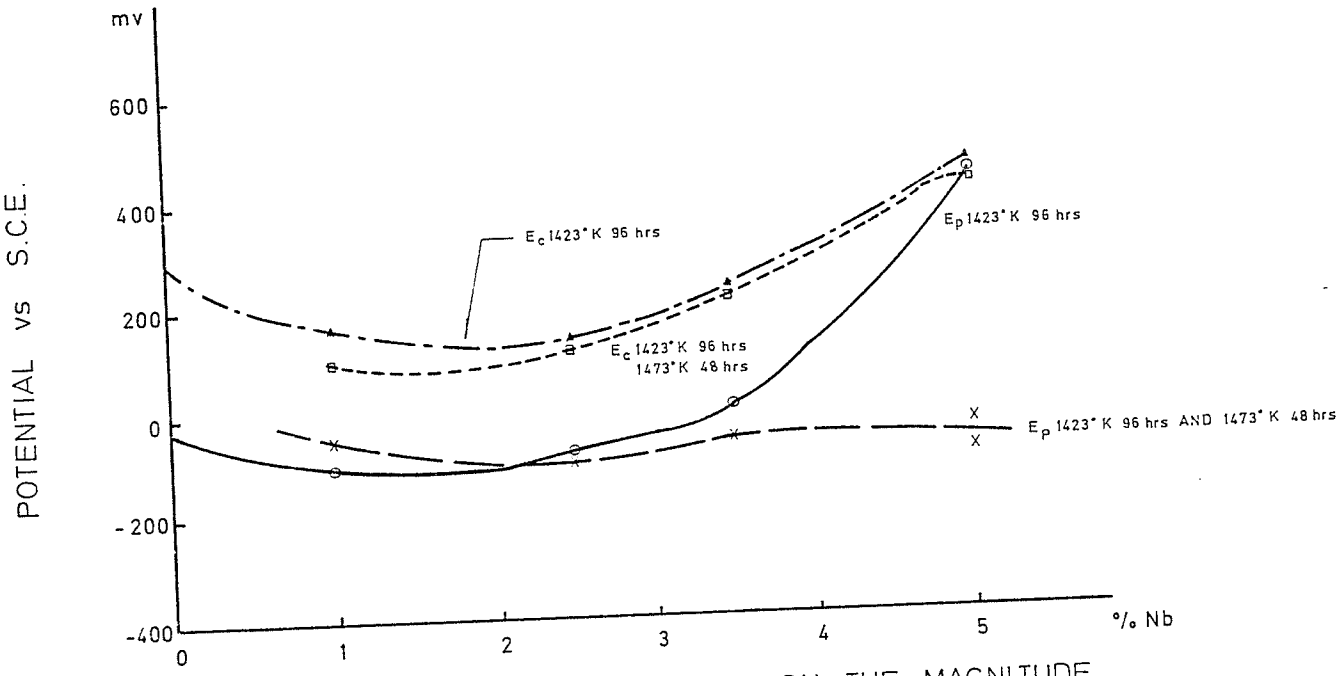

Fig. 25. EFFECT OF NIOBIUM CONTENT ON THE MAGNITUDE OF E_c AND E_p

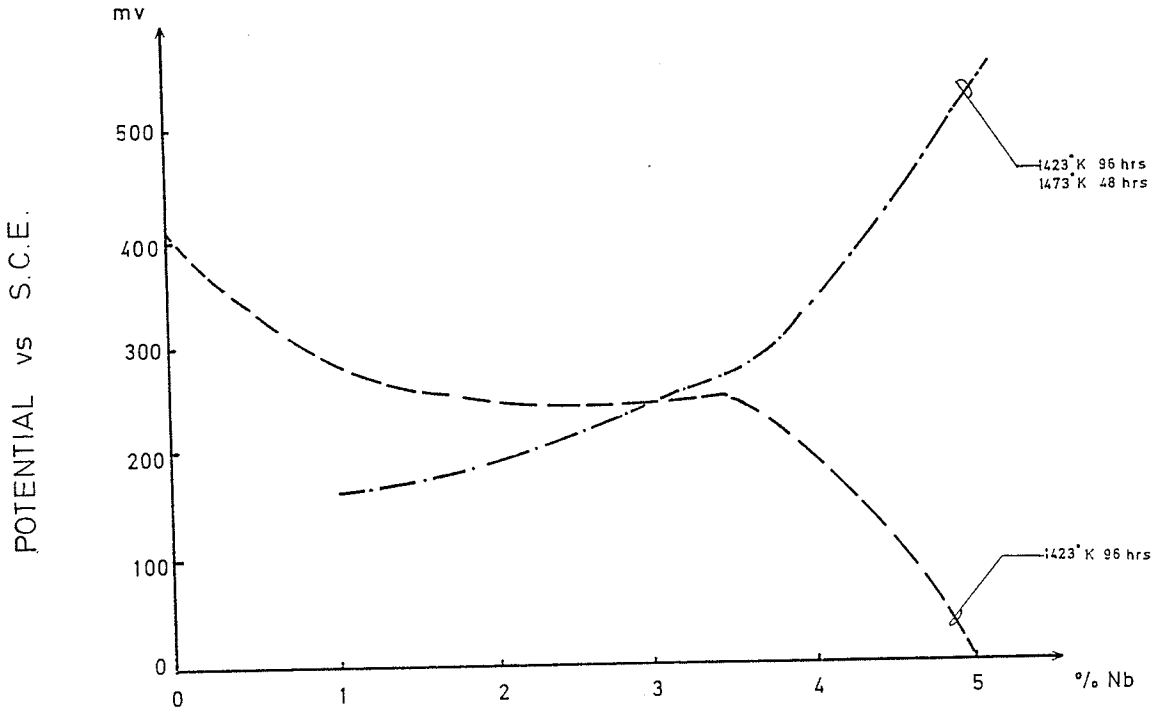

Fig. 26. EFFECT OF NIOBIUM CONTENT ON THE MAGNITUDE OF $E_c - E_p$

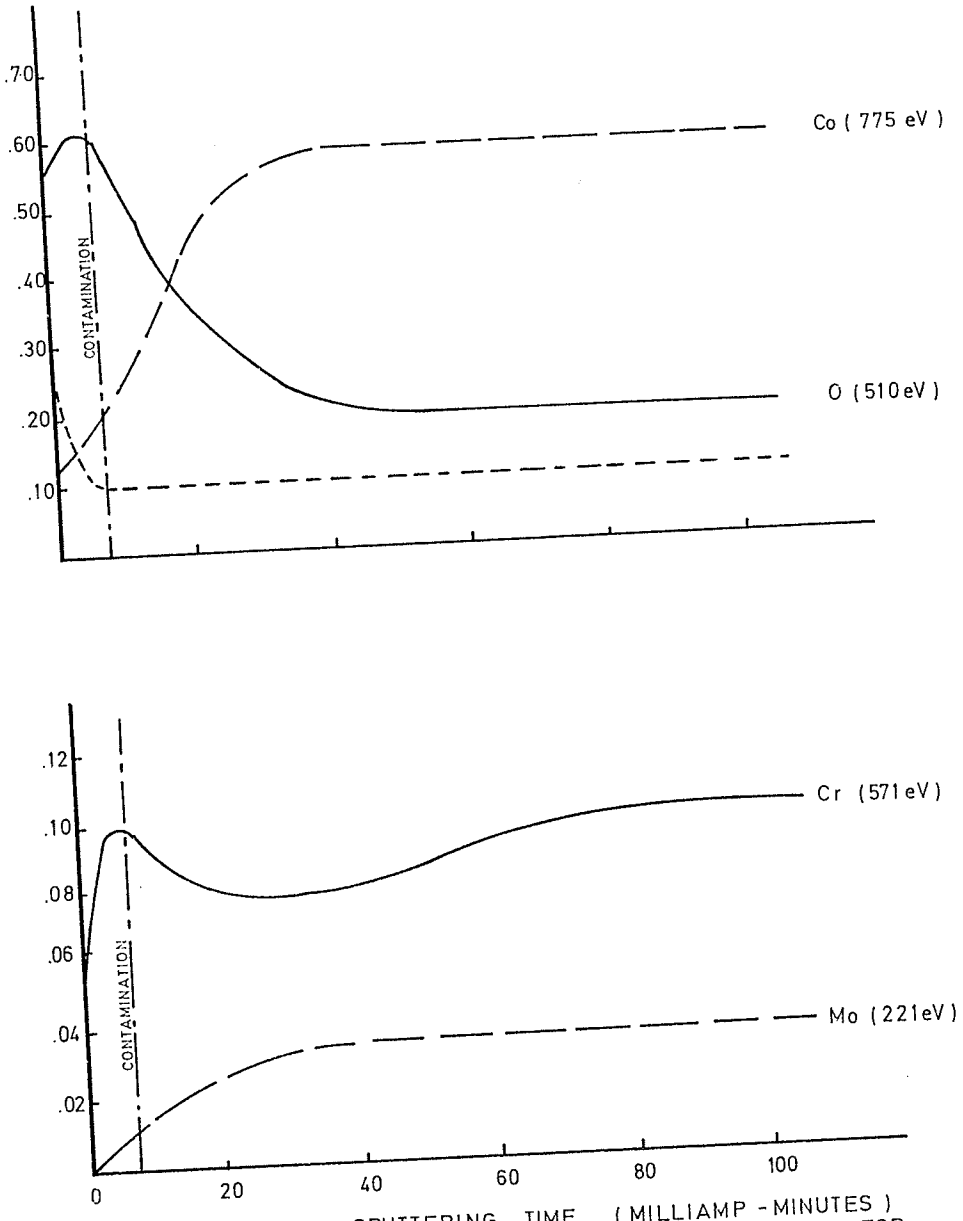

Fig. 27. NORMALIZED PEAK HEIGHTS VS SPUTTERING TIME FOR Co - 23% Cr - 2.1% Mo ALLOY

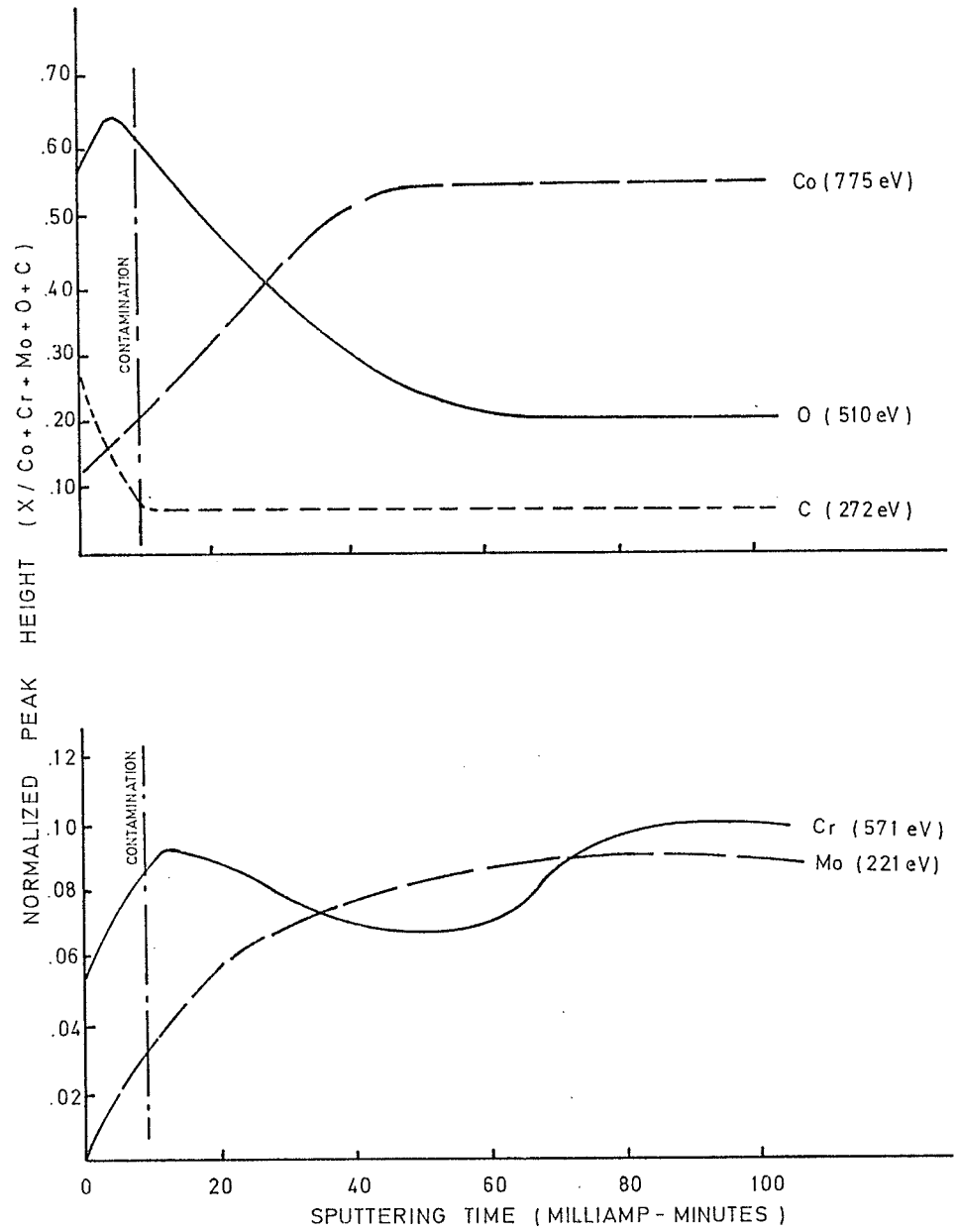

Fig. 28. NORMALIZED PEAK HEIGHTS, VS SPUTTERING TIME FOR Co - 24 % Cr - 4.7 % Mo ALLOY

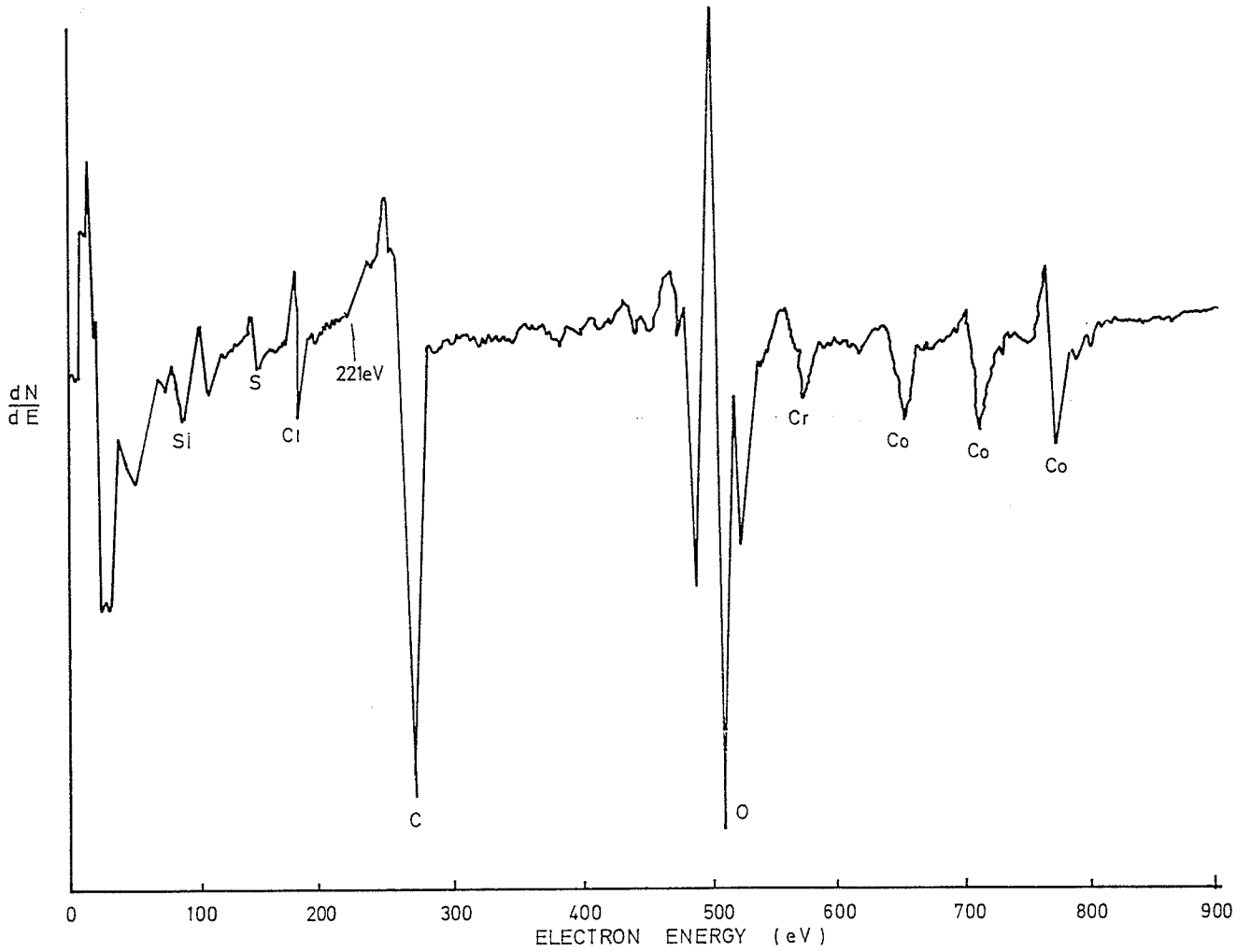

Fig. 29. SURFACE SPECTRUM PRIOR TO START OF ARGON SPUTTERING BEAM FOR Co - 24% -4.7% Mo ALLOY

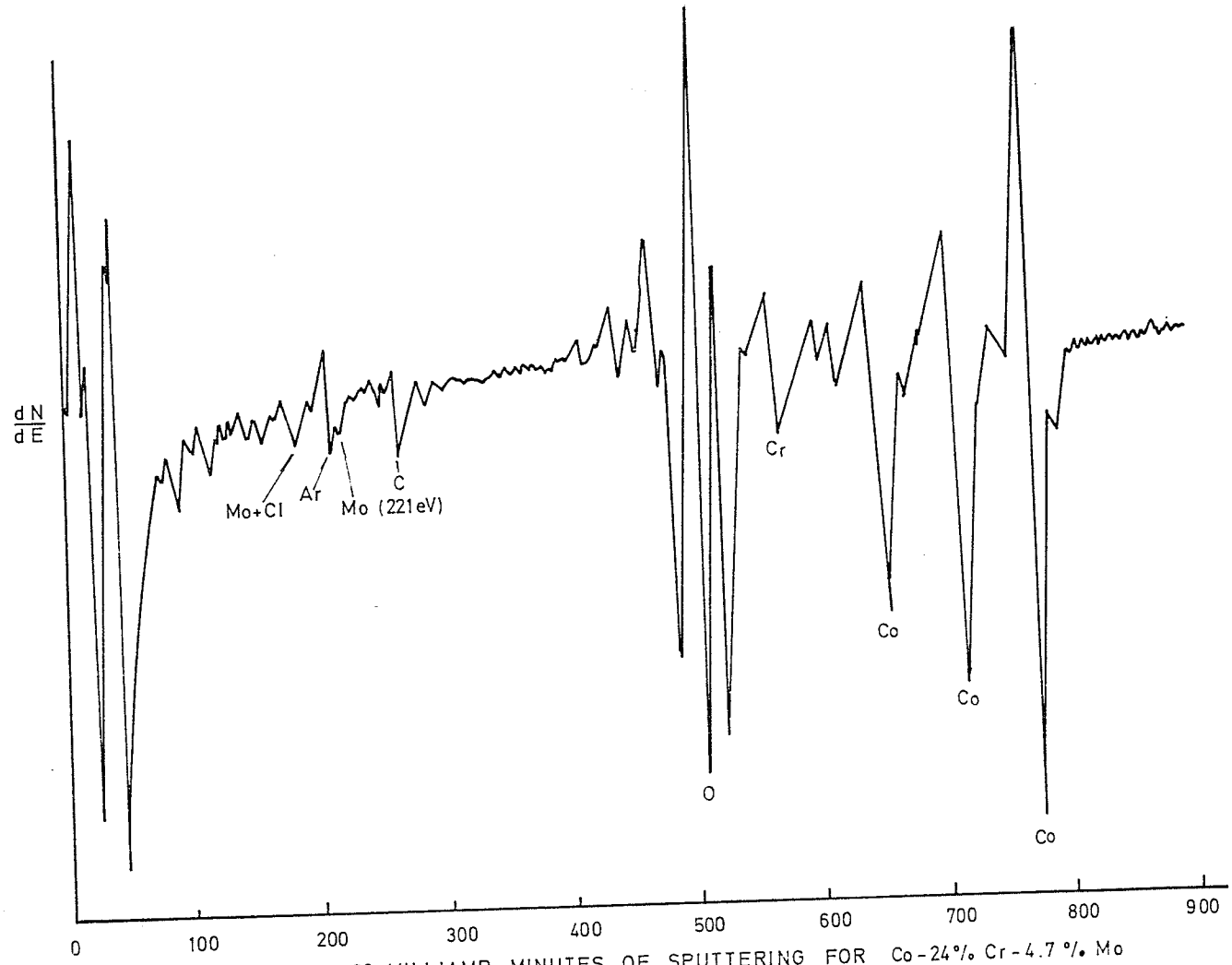

Fig. 30. SPECTRUM AFTER 28 MILLIAMP-MINUTES OF SPUTTERING FOR Co-24% Cr-4.7 % Mo

4.2 DISCUSSION

4.2.1 Effect of Mo content on corrosion behavior of Co - Cr alloy

As shown in Fig. 24 and Table II the critical potential, E_c, shifts slightly to the noble direction as the molybdenum content increases. At potential E_c, breakdown occurs on the surface film and general corrosion proceeds. It follows that the addition of molybdenum hinders the breakdown of the surface film. The hindering mechanism remains to be investigated. However, many studies have been done on the role of alloyed molybdenum on the corrosion resistance of stainless steel. M. Kolotyrkin et. al. (17) studied Fe - 18% Cr and Fe - 26% Cr with Mo contents of 0 - 1.7 atomic percent in suphuric acid at 22 C. Tests were performed in the potential region corresponding to the active state of the surface on these steels. They proposed that the inhibiting action of the Mo is achieved by the screening action of its oxides which accumulate on the surface of the steel during their dissolution. A ten-fold inhibition of the dissolution process was achieved on the production of only a fraction of a monolayer of Mo. They suggest that this inhibiting effect of a small degrees of surface coverage may be explained if the dissolution of the solid metal takes place unevenly and the largest contribution to the overall rate of this process of dissolution takes place on a relatively small number of the most active centres.

Sugimoto and Sawada (18) suggest that MoO_4^{-2} ions added to a neutral NaCl solution act effectively as a pitting inhibitor for the 20% Cr - 25% Ni steel without Molybdenum. Pit initiation and growth are both suppressed by small additions of MoO_4^{-2} ions. It was found that the added MoO_4^{-2} ions were adsorbed preferentially on the steel surface and preclude the adsorption of chloride ions. MoO_4^{-2}

T A B L E II

Figure No.	Composition Co	Cr	Mo	Nb	E_r mV	E_c mV	E_p mV	$E_c - E_p$ mV
7	Bal	26.1%	0%	0%	-310	385	- 25	410
8	Bal	25.6%	1%	0%	-218	384	8	376
9	Bal	22.8%	2.1%	0%	-290	315	52	263
10	Bal	24.8%	3.4%	0%	-286	390	390	0
11	Bal	23.8%	4.7%	0%	-244	426	426	0
12	Bal	23.1%	7.5%	0%	-237	440	440	0
14*	Bal	26%	0%	1.21%	-260	93	- 68	161
15	Bal	26%	0%	1.21%	-240	183	-110	293
16	Bal	25.2%	0%	2.2%	-213	120	Nil	Nil
17*	Bal	25.2%	0%	2.2%	-284	115	- 90	205
18*	Bal	26.4%	0%	2.75%	-180	220	- 60	280
19	Bal	26.4%	0%	2.75%	-283	225	- 28	253
20*	Bal	24.7%	0%	4.0%	-224	380	-100	480
21	Bal	24.7%	0%	4.0%	-158	420	420	0
22*	Bal	24.7%	0%	4.0%	-330	508	- 40	548
23	Bal	25%	5%	2.5%	-220	393	366	27

All of the above alloys has been heat treated at 1423 K for 96 hours before the specimens were quenched in water.

Specimens with an asterisk above were further heat treated at 1473 K for 48 hours.

film was then formed on the steel surface by the reduction of MoO_4^{-2} ions, and the film prevented the chloride attack. They also found that the alloying Mo in steel would shift the pitting potential in the noble direction. They suggest that the process of inhibition

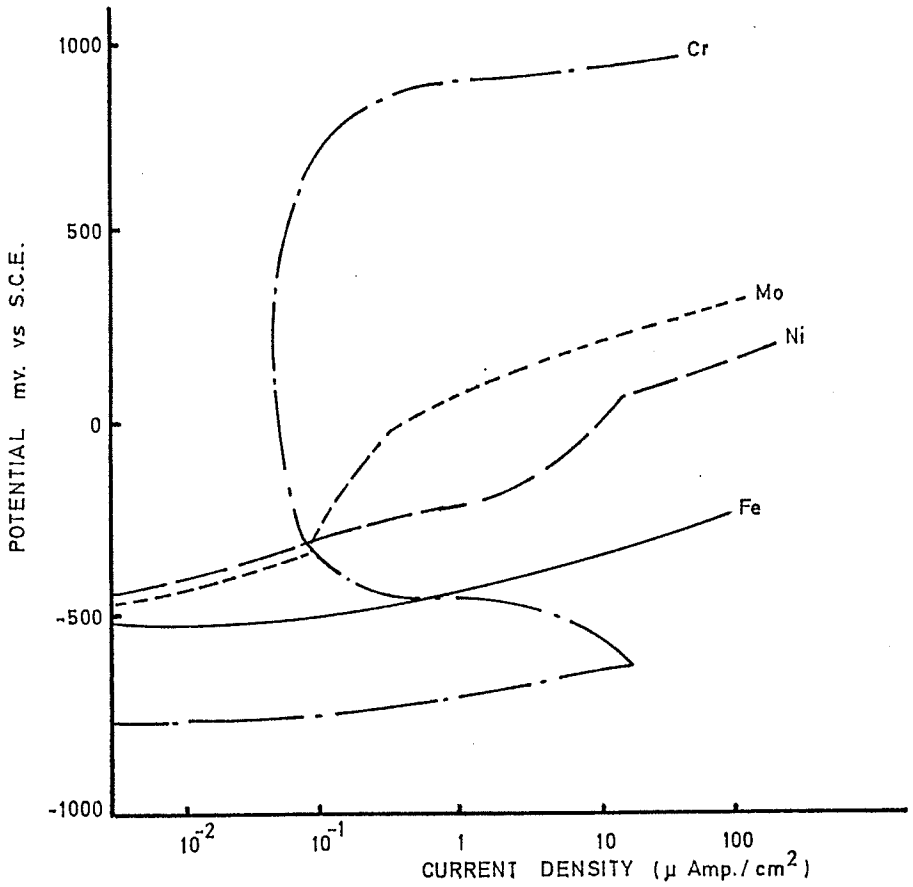

Fig. 31 Corrosion behavior of some pure metals (Ref. 19)

for the two preceding cases is somewhat common. For alloying Mo steel, MoO_4^{-2} ions go into solution during early dissolution and re-adsorption occurs on the active sites within pits at passivation stage. That is, the adsorption process of MoO_4^{-2} ions, which suppresses the pit growth is thought to be common in both methods.

Olefjord and Elfstrom (19) did some interesting work on corrosion behavior of some pure metals commonly used in stainless

steel. The solutions they employed were 0.1 M HCl and 0.4 M NaCl. The results are shown in Fig. 31. Chromium appears to have the highest breakdown potential as compared to molybdenum. Three other alloys were also tested, (1) Fe-21.7%Cr-17.3%Ni-3.6%Mo, (2) Fe-18.7%Cr-11.2%Ni-1.7%Mo, (3) Fe-18%Cr-8%Ni-0.1%Mo. The polarization curves are shown in Fig. 32. The polarization curves of the alloys show that the high Mo alloyed steel,

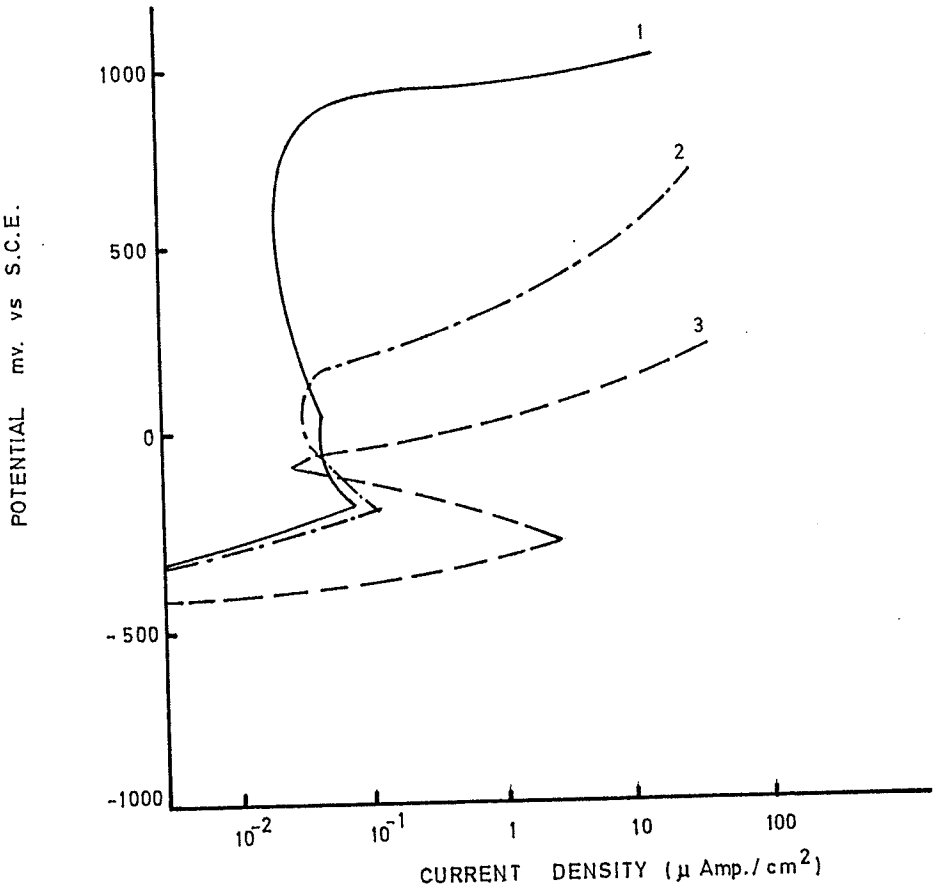

Fig. 32 Polarization curves for Mo containing stainless steel

number 1, is passive over a broad potential range. The other two alloys are sensitive to pitting corrosion above a critical potential which limits their passive range. These results are in

agreement with the results in the present investigation that the critical potential increases as Mo content increases. Although two different base alloys were employed, there is a clear indication that Mo in Co - Cr alloys and stainless steels contributes to a marked improvement of pitting resistance.

Bandy and Cahoon (20) did some polarization tests on austenitic stainless steels in Ringer's solution. They concluded that the corrosion resistance by shifting E_c in the noble direction, and Mo appears to be the most effective in imparting resistance to localized corrosion.

It has been recognized for some time that the protection potential, E_p, is one of the major indications of the polarization test. However, E_p itself is not a property of that material. The magnitude of E_p depends on the extent of the pit propagation. This effect has already been discussed in section 2.5. The significance of E_p is therefore applicable for comparison purposes if pit propagation is allowed to the same extent for all specimens. In all the potentiodynamic polarization tests here, the voltage scan was reversed at current about 100 $\mu a/cm^2$. Wilde (15) has shown that the magnitude of the "difference potential" ($E_c - E_p$) is related to the crevice corrosion weight loss. For alloys that exhibit no breakdown during a normal polarization test, the presence of hysteresis during cyclic polarization with an artificial crevice indicates susceptibility to crevice corrosion. Pourbaix et al. (21) have described the significance of E_p and demonstrated that pits initiated at potentials noble to E_c for a short period of time would continue to grow when the specimen was held at a potential between E_c and E_p. At potentials active to E_p, pits ceased to grow and the steel surface repassivated. The protection potential, E_p, as shown in Fig. 24 shifts in the noble direction as Mo content increases. This is the potential at which the existing pits start to repassivate again. It can be assumed that the same process as suggested by Sugimoto and Sawada i.e. adsorption of MoO_4^{-2}, takes place during repassivation. Again, as

the voltage scan continues in the direction more noble than E_c, general corrosion occurs. As alloying elements dissolve into the solution, MoO_4^{-2} ions can be formed. When the reverse scan starts, MoO_4^{-2} ions absorb onto the surface and repassivation occurs. Thus, the presence of Mo in Co - Cr alloys shifts both the E_c and E_p in the noble direction. For stainless steel, Wilde's experimental data (15) also show that the presence of Mo shifts both E_c and E_p in the noble direction.

The difference potential $E_c - E_p$ for all the Co - Cr - Mo alloys tested is summarized in Fig. 13. The value of $E_c - E_p$ is zero for Co - Cr alloys containing 3%, 5% and 7% of Mo. For alloys containing 0% to 2% of Mo, the value of $E_c - E_p$ progressively decreases. In summary, the presence of Molybdenum in Co - Cr alloys improves the crevice and pitting corrosion resistance of the alloy.

In order to investigate the reasons for the effect of Mo on the corrosion resistance of Co - Cr alloys, two specimens were submitted for surface analysis by Auger Electron Spectroscopy. The composition profiles for both alloys Co - 24% Cr - 4.7% Mo and Co - 23% Cr - 2.1% Mo show little effect on the overall profiles due to a decrease of Molybdenum content from 4.7% to 2.1%. Both alloys show high surface concentrations of carbon and oxygen. The carbon concentration decreases rapidly upon sputtering reaching an equilibrium value after less than 10 milliamp-minutes. The carbon concentration on the surface is likely due to contamination during handling in atmosphere and is not a part of the actual oxide film. Evidence for this is given by Bandy (22) and Cahoon and Brandy (26) who observed much lower concentrations of carbon on the surface during a second profile obtained on a different spot of the same specimen immediately following the initial profile. If the existence of carbon concentration on the surface is due to contamination, then it follows, as indicated from Figs. 27 and 28 that the oxide films for both alloys are located beneath the carbon

contaminated layer which requires about 10 milliamp-minutes of sputtering time to remove. If this is true, the oxide layer for both alloys is mainly rich in chromium and oxygen.

The chromium concentration in both alloys peaks at about 10 milliamp-minutes and gradually decreases to a minimum at about 40 to 50 milliamp-minutes. After 80 milliamp-minutes of sputtering, the Cr concentration for both alloys reached the bulk concentration. The oxygen concentration in both alloys also peaks at about 10 milliamp-minutes of sputtering time and gradually decreases to a bulk concentration after about 60 milliamp-minutes. The similar surface concentration profiles for both chromium and oxygen strongly indicates that a surface structure composed of chromium oxide is likely.

The molybdenum content on the surface of both alloys is essentially zero. Some signal of Co and Mo might have been picked up due to the atomic layers of Co and Mo underneath the oxide film. This indicates that the concentration of Mo and Co are even lower than that indicated at 10 milliamp-minutes sputtering time as shown in Fig. 27 and 28. The absence of Mo on the surface is shown in Fig. 29 where the 221 eV Mo peak is clearly absent. After 28 milliamp-minutes of sputtering, the 221 eV Mo peak can be found immediately following the 212 eV Ar peak. The 186 eV and 221 ev peaks should be essentially the same magnitude (23) and therefore the peak at 186 eV is likely due to the Mo signal.

Sugimoto and Sawada (18) analyzed the passive film of some Molybdenum containing austenitic stainless steels employing X-ray photoelectron spectroscopy. They have shown that the Mo content of the film is directly proportion to the bulk content. They suggest that the contribution of Mo content in the passive film is the cause of the improved pitting resistance of steel. However, it should be noted that they claim the surface Mo is in the hexavalent state. Auger analysis for Mo requires minitoring of

either the 186 eV or 221 eV peak, both of which involve valence electrons. Since Auger peaks from non-valence electrons are required to accurately compare surface oxide concentration with bulk concentration because of different binding energies invovled (24), the Auger results determined using valence electron peaks could be erroneous. Also, the sputtering cross-sections vary from atom to atom and depend upon its chemical environment. An unusually drastic example is the removal of equal amounts of Mo deposited on various surfaces (25): Mo forms on tungsten with a uniform film with a normal sputtering profile while on Cu, Au and Al, it agglomerates and can be observed over a range of depth. Another disturbing effect is the ion bombardment induced movement of ions on the boundaries of the film (26). These effects limit the accuracy of Auger Electron Spectroscopy and possibly lead to erroneous results of the above tests.

Olefjord and Elfstrom (19) studied the composition of the surface during passivation of stainless steel Electron Spectroscopy for Chemical Analysis (ESCA) was employed for surface analysis. Two alloys were used, (1) Fe-21.7%Cr-17.3%Ni-3.6%Mo, (2) Fe-18.7%Cr-11.2%Ni-1.7%Mo. For 3.6% Mo steel, they found the oxide film consisted of the cations of Fe, Cr and Mo. The Nickel content in the oxide was low. The dominating element in the passive film again is chromium. Molybdenum exists in more than one oxide state which depends on the polarized potential. At low potential, molybdenum exists as low valence Mo-oxide, while at a high potential (500mV), Mo is oxidized to its hexavalence state. This result agrees with that of Sugimoto and Sawada (18). Olefjord and Elfstrom also did some tests on the two alloys by polarizing them at a potential 200mV below the corrosion potential where no passive film will grow on the surface. They found that the surface of the alloy during active dissolution is enriched with the alloying elements. It was suggested that the enriched surface zone during active dissolution consists of two planes. One consisting of atoms in the oxide and the other in the outermost layer in the metal phase immediately under the oxide. The difference of concentration of

alloying elements in the surface and bulk is in the range of 20 to 30%. Their experiment showed that for 3.6%Mo steel, Cr and Ni are each enriched by a factor of 1.5, while Mo is enriched by a factor of 7 at the surface layer as compared to the bulk. For the case of polarization at a potential in the passive range, the alloy surface mainly consisted of a layer of chromium oxide and Mo was not enriched at all. They suggested that the role of Molybdenum is to stabilize the passive film and the beneficial effect is not related to its presence in the passive film. Instead, the Mo lowers the dissolution rate in the active phase and thereby provokes formation of the passive film during passivation and during local corrosive attack.

Figs. 27 and 28 show no indication of Mo enrichment at all which contradicts the result of Olefjord and Elfstrom. This is an agreement with the results of Lumsden et al (27) and Pons et al (24) who found no Mo on the surface of stainless steels using AES. However, the specimens submitted for AES test were not potentiodynamic polarized before the test. Both alloys were immersed in the 0.17M saline solution buffered with 0.034 g/l of Na_2CO_3 for 6 hours prior to surface analysis. The rest potential for 6 hours immersion for both alloys is about -300mV which is well below the breakdown potential. This could mean the rest potential is not high enough to activate the mechanism (similar to short range ordering) suggested by Olefjord and Elfstrom. However, it is interesting to note the surface depletion of Mo and Co of the two specimens. It can be assumed that the depletion of Mo and Co at the surface is mainly due to the low rest potential which causes the enrichment of Cr at the surface. It may be that the Cr is more mobile than Co and Mo under the low electrochemical potential force. The result is the trough of Cr concentration at about 40 ma minutes as shown in Figs. 27 and 28. The explanation for the effect of Mo on the polarization behavior is not immediately obvious because of the conflicting Auger and ESCA results. Further investigation of the oxide film (films built up at various potentials) is necessary for interpretation of the Mo effect.

4.2.2 Effect of Niobium content on corrosion behavior of Cobalt - Chromium alloy

The effect of Niobium content on corrosion behavior of Cobalt chromium alloy is illustrated in Figs. 25 and 26. For alloys heat treated at 1423 K for 96 hours, the values of E_c and E_p both decrease from 0 to 2% Nb content and both increase from 2 to 5% Nb content. The difference potential $E_c - E_p$ decreases from about 400 mV at 0% Nb to 0 mV at 5% Nb. For alloys given a further heat treatment at 1473 K for 48 hours, the value of $E_c - E_p$ increases as Nb content increases. However, the E_c behavior is similar for both treatments, increasing from about 160 mV at 2% Nb to about 450 mV for 5% Nb. For alloys heat treated at 1423 K for 96 hours and then 1473 K for 48 hours, the value of E_p remains at around -50 mV regardless of Nb content. Therefore, it is suggested that the presence of Nb in Co-Cr base alloys would increase the pitting potential E_c of the alloy providing that the Nb content is greater than 2 percent. For the purpose of crevice corrosion resistance, Graph 20 indicates that the 5% Nb alloy treated at 1423 K for 96 hours possesses the best crevice corrosion resistance. The value of $E_c - E_p$ for 5% Nb alloy treated at two different temperatures exhibits a difference of almost 500 mV. According to the value of $E_c - E_p$, the alloy treated at 1423 K for 96 hours, is immune to crevice corrosion. Due to the lack of information on the surface analysis of these alloys, it is hard to draw conclusions as to the mechanism of Nb on the corrosion behavior of Co - Cr base alloys. It may well be that the results obtained for the 5% Nb alloy heat treated for 96 hours at 1420 K are erroneous and that Nb had little effect at all on the corrosion behavior of Co-25% Cr alloys.

A Co-25%Cr-2.5%Nb-5%Mo alloy was also tested and the result is shown in Fig. 23. Both the E_c and E_p for this alloy are more active than the E_c and E_p of Co-25%Cr-5%Mo. Also, the $E_c - E_p$ for 2.5%Nb-5%Mo is 27 mV while the value for 5%Mo alloy is zero. This means the addition of 2.5%Nb to the 5%Mo alloy increases slightly the susceptibility to crevice corrosion.

4.2.3 Observation from microstructure

The microstructures of the 0 to 7%Mo Co-Cr alloys are shown in Figs. 33 to 37. For alloys contain 1 to 5%Nb, the microstructures are shown from Figs. 38 to 46, the microstructure of Co-Cr-5%Mo-2.5%Nb is shown in Fig. 47.

For Nb containing alloys, the effect of heat treatment is not obvious as far as microstructure is concerned. The variation of Mo and Nb contents in Co-Cr alloys seems to have little or no effect on the microstructure. It is well known that the addition of Mo in Co-Cr alloys will strengthen the alloys considerably. In Co-Cr-Mo alloys, the matrix is HCP at 1073 K and FCC at 1273 K. For the alloys tested here it was confirmed by X-ray diffraction that the structure was a mixture of HCP and FCC. The microstructures are composed mainly of twinned grains with dispersed impurity carbides. This is expected for alloys quenched in water from temperature of 1423 K.

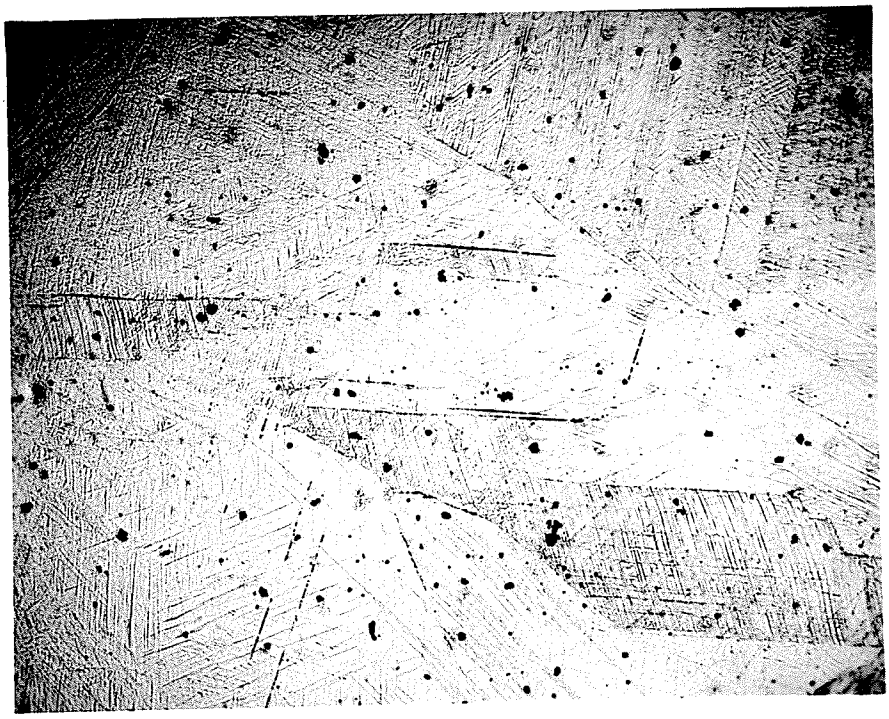

Fig. 33 Co - 25%Cr X100 1423 K 96 hrs.

Fig. 34 Co - 25%Cr - 1%Mo X100 1423 K 96 hrs.

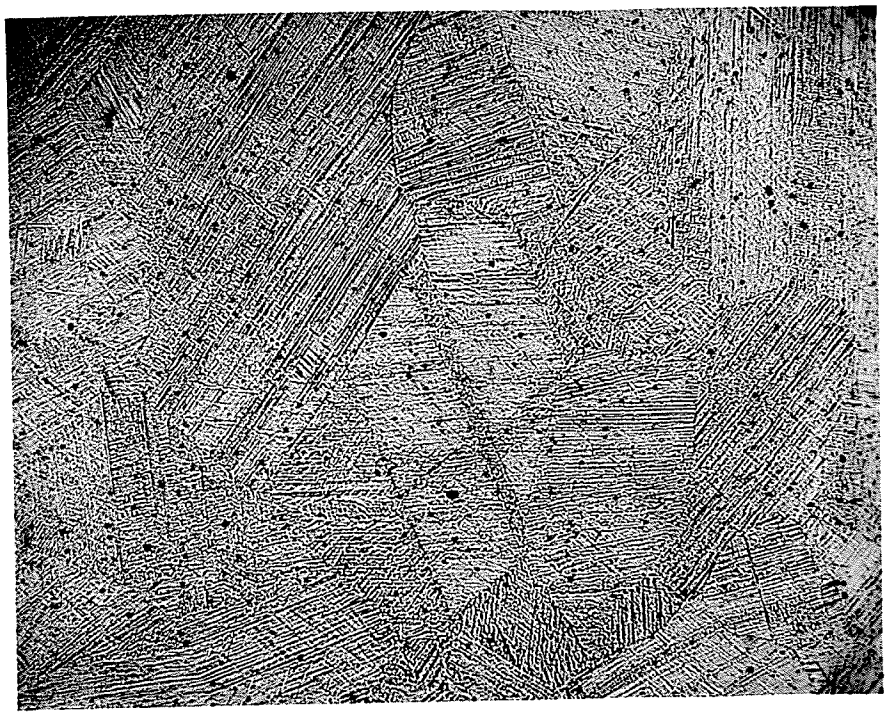

Fig. 35 Co - 25%Cr - 2%Mo X100
1423 K 96 hrs.

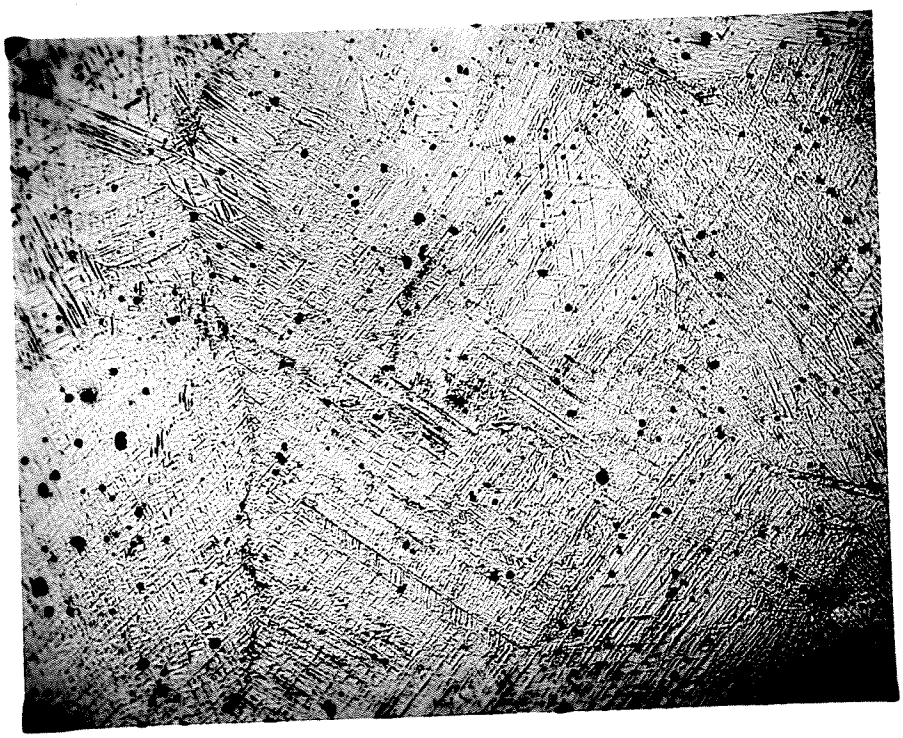

Fig. 36 Co - 25%Cr - 3%Mo X100
1423 K 96 hrs.

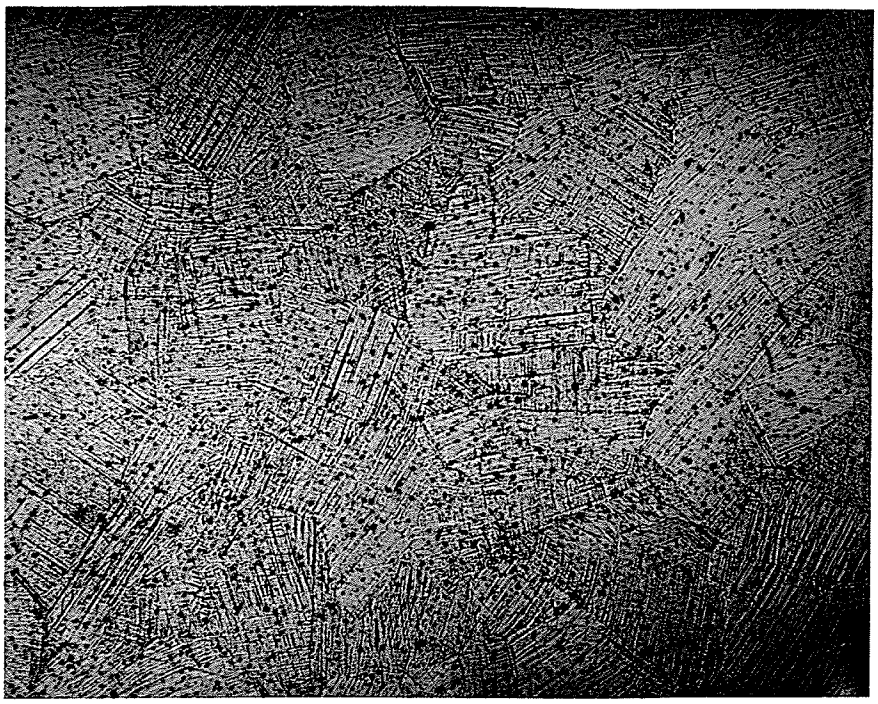

Fig. 37 Co - 25%Cr - 7%Mo X100
1423 K 96 hrs.

Fig. 38 Co - 25%Cr - 1%Nb X300
1423 K 96 hrs. 1473 K 48 hrs.

Fig. 39 Co - 25%Cr - 1%Nb X350
1423 K 96 hrs.

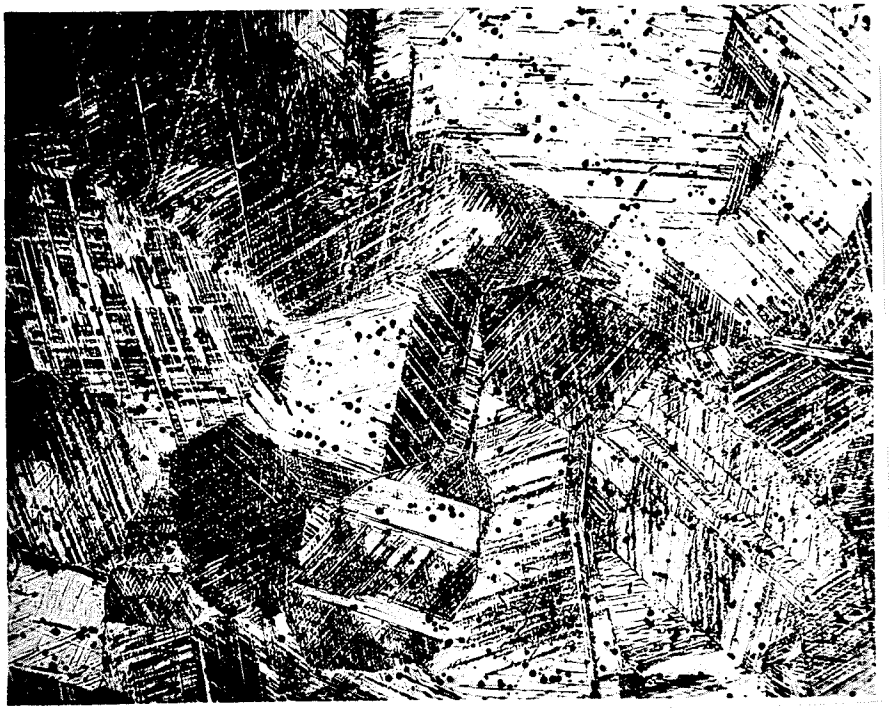

Fig. 40 Co - 25%Cr - 2.5%Nb X100
1423 K 96 hrs.

Fig. 41 Co - 25%Cr - 2.5%Nb X100
1423 K 96 hrs. 1473 K 48 hrs.

Fig. 42 Co - 25%Cr - 3.5%Nb X100
1423 K 96 hrs.

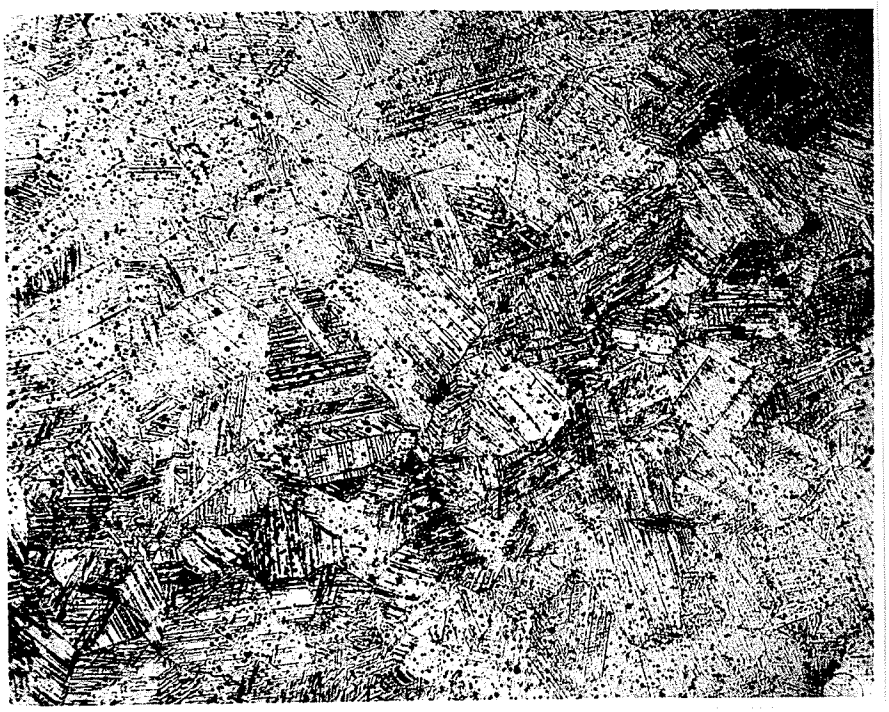

Fig. 43 Co - 25%Cr - 3.5%Nb X100
1423 K 96 hrs. 1473 K 48 hrs.

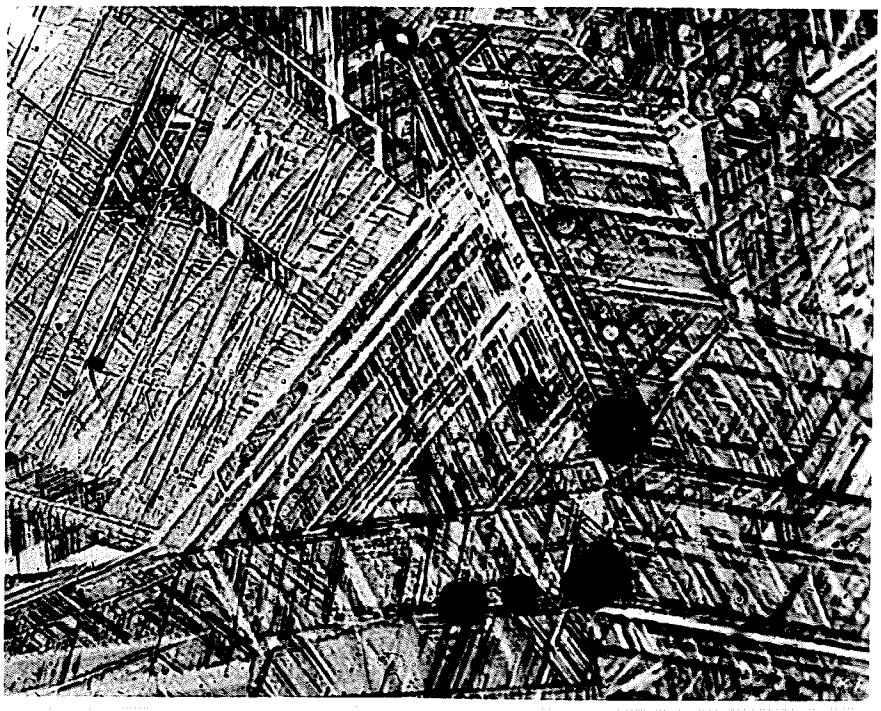

Fig. 44 Co - 25%Cr - 5%Nb X1300
1423 K 96 hrs.

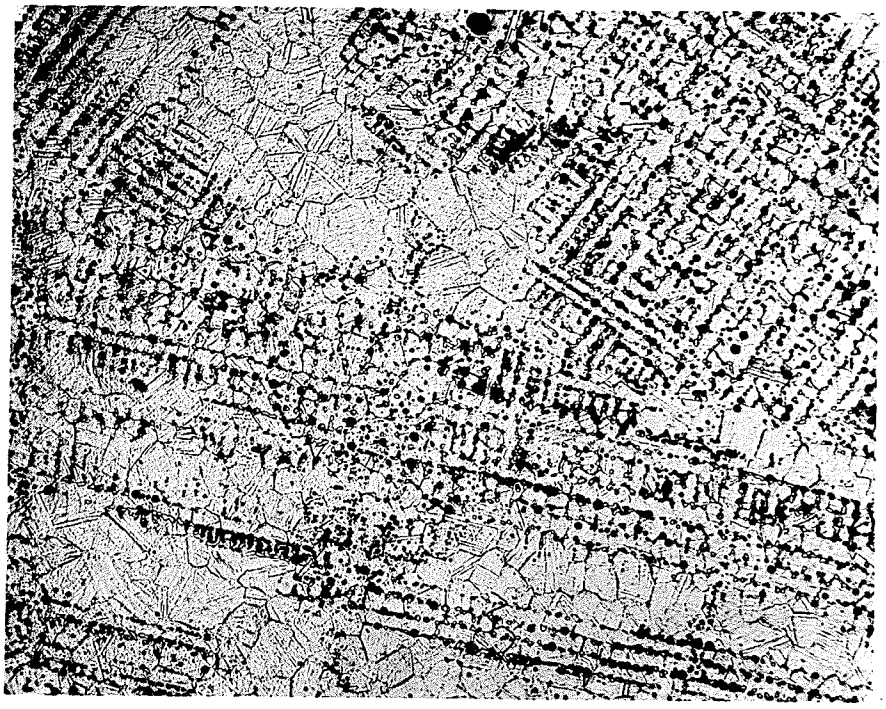

Fig. 45 Co - 25%Cr - 5%Nb X100
1423 K 96 hrs.

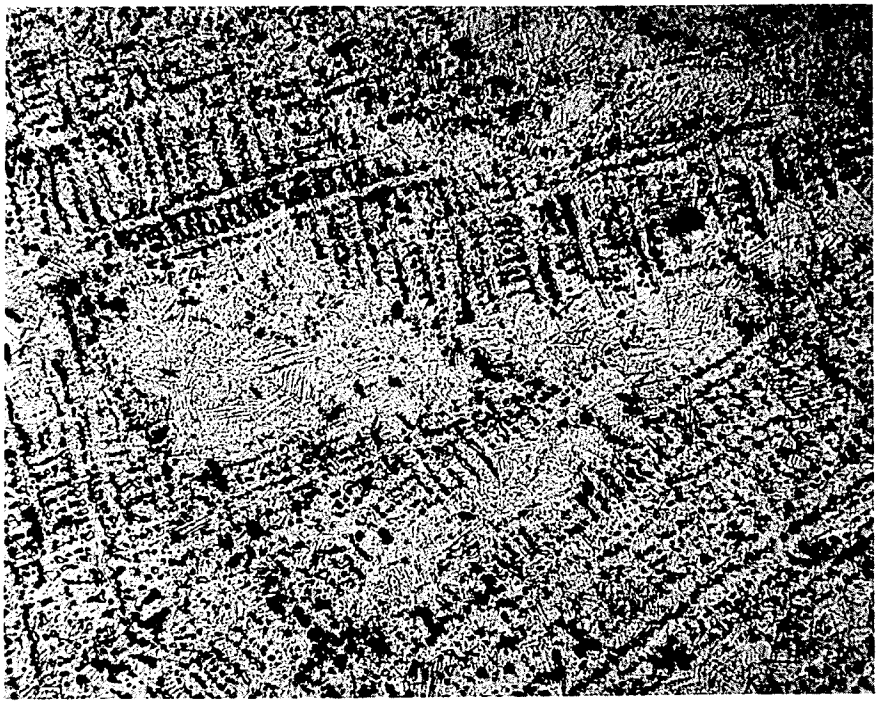

Fig. 46 Co - 25%Cr - 5%Nb X100
1423 K 96 hrs. 1473 K 48 hrs.

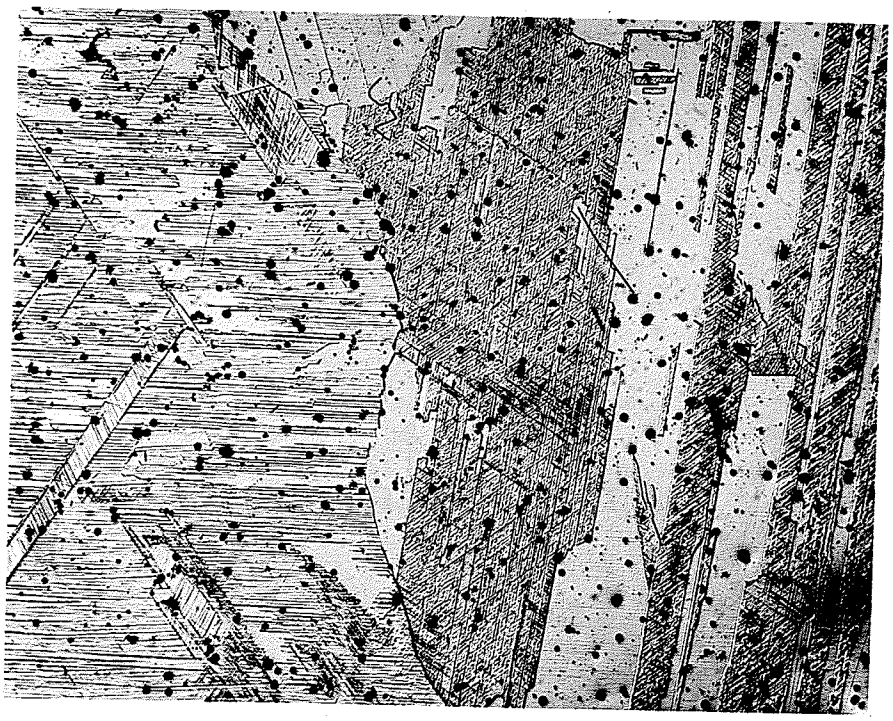

Fig. 47 Co - 25%Cr - 5%Mo - 2.5%Nb X100
1423 K 96 hrs.

4.3 Conclusions

The presence of Mo in Co base Cr alloy has a beneficial effect on the corrosion resistance of the alloy. Both the pitting corrosion and crevice corrosion resistance increases with the increase of molybdenum content in the alloy. The optimum corrosion resistance requires 3 or more wt. % Mo. Co base Cr alloys containing less than 2% Mo are susceptible to crevice corrosion in physiological environment.

The exact reasons for the beneficial effect of Mo on the corrosion resistance of Co base Cr alloys remains to be investigated. The results of Auger Analysis give no indication as to the presence of Mo in the oxide film nor the enrichment of Mo on the metal surface. Further study is suggested on alloys polarized at high potentials near the critical potential.

The effect of Nb on the corrosion behavior of Co base Cr alloys is not clear. However, the presence of Nb up to 4% or 5% increases slightly the critical potential or the pitting potential. Heat treatment temperature seems to have some effect on the E_p of the 5%Nb alloy. Co-25%Cr-5%Nb heat treated at 1423 K for 96 hours seem to be immune from crevice corrosion in physiological environment while the same alloy treated an extra 48 hours at 1473 K is highly susceptible. Further investigation is necessary for clarification.

LIST OF REFERENCES

1. Biomedical Materials in Surgery, Annual Review of Material Science, 1974, 4, p. 415

2. Biomedical Materials in Surgery, Annual Review of Material Science, 1974, 4, p. 417

3. T. M. Devine and J. Wulff, Cast vs. Wrought Cobalt-Chromium Surgical Implant alloys, Journal of Biomedical Material Research, Vol. 9, pp. 151-167 (1975)

4. Fontana & Greene, 'Corrosion Engineering', McGraw-Hill, p. 42 (1978)

5. M. A. Genshaw, 'Electrosorption' edited by Eliezer Gileadi, Plenum Press, New York, (1967), pp. 76-85

6. Lanyon and Trapnell, Proc. Roy. Soc. A227, 387 (1955)

7. Jerome Kruger, 'Passivity and its breakdown on iron and iron base alloys', U.S.A. - Japan seminars, NACE, pp. 91-98 (1976)

8. J. A. Richardson and G. C. Wood, Journal of Electrochemical Society, Vol. 120, p. 193 (1973)

9. J. A. Richardson and G. C. Wood, Corrosion Science, Vol. 10, p. 313 (1970)

10. T. P. Hoar, D. C. Mears and G. P. Rothwell, Corrosion Science, Vol. 5, p. 279 (1965)

11. T. P. Hoar, Corrosion Science, Vol. 7, p. 355 (1967)

12. N. Sato, Electrochemica Acta, Vol. 19, p. 1683 (1971)

13. J. Kruger and J. R. Ambrose, NBS Report NBSIR, pp. 74-583, September (1974)

14. B. E. Wilde and E. Williams, "The use of Current/Voltage curves for the study of Localized Corrosion and Passivity Breakdown on Stainless Steels in Chloride media', submitted for publication in Electrochemica Acta as part of the Proceedings of the 3rd International Conference of Passivity, Cambridge, England, July 1970

15. B. E. Wilde, Corrosion, Vol. 28, No. 8, August 1972

16. "Standard recommended practice for standard reference method for making potentiostatic and potentiodynamic anodic polarization measurements", ASTM 1978, pp. 816-826, G5

17. M. Kolotyrkin, et. al. 'The influence of Mo on corrosion properties of stainless steel', Metal Abstract, January 1980, Vol. 13, Pt. 1, Abstract no. 35-0048

18. Katsuhisa Sugimoto and Yoshinobu Sawada, Corrosion, Vol. 32, No. 9, September 1976, pp. 347-352

19. Ingemar Olefjord and Bengt-Olof Elfstrom, Corrosion, Vol. 38, No. 1, January 1982, pp. 46-52

20. R. Bandy and J. R. Cahoon, Corrosion, Vol. 33, No. 6, June 1977, pp. 204-208

21. M. Pourbaix, et. al., Corrosion Science, 3, 239 (1963)

22. R. Bandy, Ph. D. Thesis, University of Manitoba, February 1976

23. P. W. Palmberg, G. E. Reach, R. E. Weber and N. C. Macdonald, Handbook of Auger Electron Spectroscopy, Physical Electronic Industries, Minnesota, p. 81, 1972

24. R. Pons, J. Leherichy and J. P. Langeron, Surface Science, Vol. 69, pp. 547-564, 1977

25. M. L. Tarng, G. K. Wehner, Journal of Applied Physics, Vol. 43, p. 2268, 1972

26. J. R. Cahoon and R. Bandy, Corrosion, Vol. 30, (6), pp. 299-305, (1982)

27. J. B. Lumsden and R. W. Staehle; Scripter Met, Vol. 6, pp. 1205-1208, 1972